African Swine Fever Virus and host response - transcriptome profiling of the Georgia 2007/1 strain and porcine macrophages

Gwenny Cackett[a§], Raquel Portugal[b§] , Dorota Matelska[a], Linda Dixon[b*] and Finn Werner*[a]

[a]Institute for Structural and Molecular Biology, Darwin Building, University College London, Gower Street, London WC1E 6BT, United Kingdom

[b]Pirbright Institute, Ash Road, Pirbright, Surrey, GU24 0NF, United Kingdom

[§] have contributed equally to this work

Short Title:

The ASFV Georgia 2007/1 Strain Transcriptome

#Address correspondence to linda.dixon@pirbright.ac.uk and f.werner@ucl.ac.uk.

Abstract [222 words]

African swine fever virus (ASFV) has a major global economic impact. With a case fatality in domestic pigs approaching 100%, it currently presents the largest threat to animal farming. Although genomic differences between attenuated and highly virulent ASFV strains have been identified, the molecular determinants for virulence at the level of gene expression have remained opaque. Here we characterise the transcriptome of ASFV genotype II Georgia 2007/1 (GRG) during infection of the physiologically relevant host cells, porcine macrophages. In this study we applied Cap Analysis Gene Expression sequencing (CAGE-seq) to map the 5' ends of viral mRNAs at 5 and 16 hours post-infection. A bioinformatics analysis of the sequence context surrounding the transcription start sites (TSSs) enabled us to characterise the global early and late promoter landscape of GRG. We compared transcriptome maps of the GRG isolate and the lab-attenuated BA71V strain that highlighted GRG virulent-specific transcripts belonging to multigene families, including two predicted MGF 100 genes I7L and I8L. In parallel, we monitored transcriptome changes in the infected host macrophage cells. Of the 9,384 macrophage genes studied, transcripts for 652 host genes were differentially regulated between 5 and 16 hours-post-infection compared with only 25 between uninfected cells and 5 hours post-infection. NF-kB activated genes and lysosome components like S100 were upregulated, and chemokines such as CCL24, CXCL2, CXCL5 and CXCL8 downregulated.

Importance [183 words]

African swine fever virus (ASFV) causes haemorrhagic fever in domestic pigs with case fatality rates approaching 100%, and no approved vaccines or antivirals. The highly-virulent ASFV Georgia 2007/1 strain (GRG) was the first isolated when ASFV spread from Africa to the Caucasus region in 2007. Then spreading through Eastern Europe, and more recently across Asia. We used an RNA-based next generation sequencing technique called CAGE-seq to map the starts of viral genes across the GRG DNA genome. This has allowed us to investigate which viral genes are expressed during early or late stages of infection and how this is controlled, comparing their expression to the non-virulent ASFV-BA71V strain to identify key genes that play a role in virulence. In parallel we investigated how host cells respond to infection, which revealed how the ASFV suppresses components of the host immune response to ultimately win the arms race against its porcine host.

Introduction [1,317 words]

ASFV originated in Sub-Saharan Africa where it remains endemic. However, following the introduction in 2007, of a genotype II isolate to Georgia (1), and subsequent spread in Russia and

44 Europe. The virus was then introduced to China in 2018 (2), from here it spread rapidly across Asia,
45 strongly emphasizing this disease as a severe threat to global food security. ASFV is the only
46 characterised member of the Asfarviridae family (3) in the recently classified Nucleocytoviricota
47 (ICTV Master Species List 2019.v1) phylum (4,5). ASFV has a linear double-stranded DNA (dsDNA)
48 genome of ~170–193 kbp encoding ~150–~200 open reading frames (ORFs). Until recently, little was
49 known about either the transcripts expressed from the ASFV genome or the mechanisms of ASFV
50 transcription. Much of what is known about transcription is extrapolated from vaccinia virus (VACV),
51 a distantly-related Nucleocytoviricota member, from the Poxviridae family (6). ASFV encodes a
52 eukaryotic-like 8-subunit RNA polymerase (RNAP), an mRNA capping enzyme and poly-A
53 polymerase, all of which are carried within mature virus particles (7). These virions are transcription
54 competent upon solubilisation in vitro (8) and support mRNA modification by including a 5'-
55 methylated cap and a 3' poly-adenylated (polyA) tail of ~33 nucleotide-length (8,9).

56 Viral genes are typically classified according to their temporal expression patterns - ASFV genes have
57 historically been categorised as 'immediate early' when expressed immediately following infection,
58 as 'early genes' following the onset of viral protein synthesis, as 'intermediate genes' after the onset
59 of viral DNA replication, or as 'late genes' thereafter. The temporal regulation of transcription is
60 likely enabled by different sets of general transcription initiation factors that recognise distinct early
61 or late promoter motifs (EPM or LPM, respectively), as we previously investigated in the ASFV-BA71V
62 strain (10), and address further in this study. EPM recognition is likely enabled by the ASFV
63 homologue of heterodimeric VACV early transcription factor (VETF), consisting of D1133L (D6) and
64 G1340L (A7) gene products, which bind the Poxvirus early gene promoter motif (11–13), which the
65 ASFV EPM strongly resembles. Both ASFV-D6 and ASFV-A7 are late genes, i.e. synthesised late during
66 infection (10) and packaged into virus particles (7). The ASFV LPM is less well defined than the EPM,
67 but a possible initiation factor involved in its recognition is the ASFV-encoded viral homolog of the
68 eukaryotic TATA-binding protein (TBP), expressed during early infection (10). By analogy with the
69 VACV system, additional factors including homologs of A1, A2 and G8 may also contribute to late
70 transcription initiation (6)

71 We have recently carried out a detailed and comprehensive ASFV whole genome expression analysis
72 using complimentary next-generation sequencing (NGS) results and computational approaches to
73 characterise the ASFV transcriptome following BA71V infection of Vero cells at 5 hpi and 16 hpi post-
74 infection (hpi) (10). Most of our knowledge about the molecular biology of ASFV, including gene
75 expression, has been derived from cell culture-adapted, attenuated virus strains, such as BA71V
76 infecting Vero tissue culture cells (9,10). These model systems provide convenient models to study

77 the replication cycle but have deletions of many genes that are not essential for replication, but have
78 important roles in virulence within its natural porcine hosts. (14–16). To date 24 ASFV genotypes
79 have been identified in Africa (16–23), while all strains spreading across Asia and Europe belong to
80 the Type II genotype. Most of these are highly virulent in domestic pigs and wild boar, including the
81 ASFV Georgia 2007/1 (GRG) (24), and the Chinese ASFV Heilongjiang, 2018 (Pig/HLJ/18) (25) isolates.
82 Though a number of less virulent isolates have been identified in wild boar in the Baltic States and
83 domestic pigs in China (26–29). It is crucial to understand the similarities and commonalities
84 between ASFV strains, and to characterise the host response to these in order to understand the
85 molecular determinants for ASFV pathogenicity. Information about the gene content and genome
86 organisation can be gained from comparing virus genome sequences. However, only functional
87 genomics such as transcriptome or proteome analyses can provide information about the
88 differences in gene expression programmes and the host responses to infection.

89 On the genome level, most differences between virulent (e.g. GRG) and attenuated (e.g. lab-
90 attenuated BA71V) ASFV strains reside towards the genome termini. Figure 1a shows a whole
91 genome comparison of GRG (left) and BA71V (right) strains with the sequence conservation colour
92 coded in different shades of blue. The regions towards the ends of the genome are more dynamic
93 compared to the central region which is highly conserved, as genes at the termini are prone to
94 deletion, duplication, insertion, and fusion (17,30). Most of the GRG-specific genes are expressed
95 early during infection (early genes are colour coded blue in the outer arch of Figure 1a) and many
96 belong to Multi-Gene Families (MGFs, purple in the inner arch). The functions of many MGF
97 members remain poorly understood, though variation among MGFs is linked to virulence (31) and
98 deleting members of MGF 360 and 505 families has been shown to reduce virulence (32,33).
99 Deletion of MGF 505-7R or MGF 110-9L also partially attenuated the virus in pigs (34,35). In contrast
100 deletion of MGF 110-1L and MGF 100-1R did not reduce virus virulence (17). Members of MGF 110
101 are highly expressed both on the mRNA and protein level in infections with the BA71V isolate or
102 OURT88/3 (10,36), suggesting MGF 110 holds importance during infection. Overall, the functions of
103 MGF 360 and 505 members are better characterised than other MGFs, playing a role in evading the
104 host type I interferon (IFN) response (15,32,37–40). In summary, comparing the expression of ASFV
105 genes, especially MGFs, between the virulent GRG- and the lab adapted BA71V strains, is
106 fundamental in identification of virulence factors and better MGF characterisation.

107 Macrophages are the primary target cells for ASFV, they are important immune effector cells that
108 display remarkable plasticity allowing efficient response to environmental signals (41). There are
109 some studies which have investigated how host macrophages respond to infection, including a

110 microarray analysis of primary swine macrophage cells infected with virulent GRG (42). There are
111 two RNA-seq studies of whole blood or tissues isolated from pigs post-mortem, which were infected
112 with either a low pathogenic ASFV-OURT 88/3 or ASFV-GRG (43), or infected with a pathogenic
113 Chinese isolate ASFV-SY18 (44). Recently, two reports have been published about the transcriptomic
114 response of porcine macrophages to infection with a virulent Chinese genotype II isolate using a low
115 multiplicity of infection (MOI: 1) and classical RNA-seq (45,46), but due to different experimental
116 conditions the varying results are somewhat challenging to compare with other studies. It must also
117 be remembered that neither these classical RNA-seq nor microarray analyses, have sufficient
118 resolution to accurately capture viral gene expression in the compact ASFV genome alongside that of
119 the host.

120 Here we applied CAGE-seq to characterise the transcriptome of the highly virulent GRG isolate (24),
121 in primary porcine macrophages, the biologically relevant target cells for ASFV infection. In this study
122 we used a high multiplicity of infection (MOI: 5), so that transcripts expressed during a single cycle
123 time course could be measured without the complication of variable proportions of uninfected cells
124 being present. We investigated the differential gene expression patterns of viral mRNAs at early and
125 late time points of 5- and 16 hpi, and mapped the viral promoter motifs. Importantly, we have
126 compared the expression levels and temporal regulation of genes conserved in both the virulent
127 GRG isolate, and attenuated tissue-culture adapted BA71V strain. With a few exceptions, both mRNA
128 expression levels and temporal regulation of the conserved genes are surprisingly similar. This
129 confirms that it is not deregulation of their conserved genes, but the virulent isolate-specific genes,
130 which are the key determinants for ASFV virulence. Most of these genes are MGF members, likely
131 involved in suppression of the host immune-response. Indeed, transcriptome analysis of the porcine
132 macrophages upon GRG infection reflects a modulation of host immune response genes, although
133 the bulk of the ~ 9000 genes studied did not significantly change expression levels during infection.

134 Results [4,633 words]

135 Genome-wide Transcription Start Site-Mapping

136 We infected primary porcine alveolar macrophages with ASFV GRG at a high multiplicity of infection
137 (MOI 5.0), isolated total RNA at 5 hpi and 16 hpi and sequenced using CAGE-seq (Supplementary
138 Table 1a). The resulting mRNA 5' ends were mapped to the GRG genome (Figure 1b) resulting in the
139 annotation of 229 and 786 TSSs at 5 and 16 hpi, respectively (Figure 1c and d, from Supplementary
140 Table 1b and c, respectively). The majority of TSSs were identified within 500 bp upstream of the
141 start codon of a given ORF, a probable location for a *bona fide* gene TSS. The strongest and closest

142 TSSs upstream of ORFs were annotated as 'primary' TSS (pTSS, listed in Supplementary Table 1d) and
143 in this manner we could account TSS for 177 out of 189 GRG ORFs annotated in the FR682468.1
144 genome. TSSs signals below the threshold for detection included MGF_110-11L, C62L, and E66L, the
145 remainder being short ORFs designated as 'ASFV_G_ACD', predicted solely from the FR682468
146 genome sequence (24). The E66L ORF was originally predicted from only the BA71V genome
147 sequence, but likewise was undetectable with CAGE-seq (10), making its expression unlikely. Our TSS
148 mapping identified novel ORFs (nORFs) downstream of the TSS, which were included in the curated
149 GRG genome map (Supplementary Table 1d includes pTSSs of annotated ORFs and nORFs in gene
150 feature file or 'GFF' format). In addition to ORF-associated TSSs, some were located within ORFs
151 (intra-ORF or ioTSS), or in between them (inter-ORF TSS), and all detected TSSs are listed in
152 Supplementary Table 1b-c.

153 Expression of GRG genes during Early and Late Infection

154 Having annotated TSSs across the GRG genome, we quantified the viral mRNAs originating from
155 pTSSs from CAGE-seq data, normalising against the total number of reads mapping to the ASFV
156 genome (i. e. RPM or reads per million mapped reads per sample). We compared gene expression
157 between early and late infection, and simplistically defined genes as 'early' or 'late' if they are
158 significantly down- or upregulated (respectively), using DESeq2 (47). In summary, 165 of the 177
159 detectable genes were differentially expressed (adjusted p-value or padj < 0.05, Supplementary
160 Table 1e). Those showing no significant change were D345L, DP79L, I8L, MGF_100-1R, A859L,
161 QP383R, B475L, E301R, DP63R, C147L, and I177L. 87 of those 165 differentially expressed genes
162 were significantly downregulated, thus representing the 'early genes', while 78 of the 165 genes
163 were upregulated or 'late genes'. The majority of MGFs were early genes, apart from MGF 505-2R,
164 MGF 360-2L and MGF 100-1L (Figure 2a). Figure 2b shows the expression patterns of GRG-
165 exclusively expressed genes, which we defined as only having a detectable CAGE-seq TSS in GRG,
166 and not in BA71V (regardless of presence in the BA71V genome). These unsurprisingly, consist of
167 many MGFs (19), all of which were early genes (Figure 2b), barring MGF 100-1L. In addition genes
168 I9R, I10L and I11L and several of the newly annotated short ORFs were specific to GRG.

169 We extracted the top twenty most highly expressed genes of GRG (as RPM) during 5 hpi (Figure 2c)
170 and 16 hpi (Figure 2d) post-infection. Ten genes are shared between both top 20 lists: MGF 110-3L,
171 A151R, MGF 110-7L, MGF 110-5L-6L, I73R, 285L, CP312R, ASFV_G_ACD_00600, MGF 110-4L, and
172 CP204L. It is important to note that the relative expression values (RPM) for genes at 5 hpi are
173 significantly higher than those at 16 hpi. This is consistent with our observations in the BA71V strain
174 (10) and due to the increase in global viral transcript levels during late infection discussed below.

175 Supplementary Table 1f includes all the GRG annotated ORFs, their TSS locations during early and
176 late infection, their relative distances if these TSS locations differ, and their respective 5'
177 Untranslated Region (UTR) lengths.

178 GRG and BA71V Share Strong Similarity between Conserved Gene Expression

179 Next we carried out a direct comparison of mRNA levels from 132 conserved genes between the
180 virulent GRG and attenuated BA71V (10) strain making use of our previously published CAGE-seq
181 data. The relative transcript levels (RPM) of the genes conserved between the two strains showed a
182 significant correlation at 5 hpi (Figure 3a) and 16 hpi (Figure 3b), supported by the heatmap in
183 Supplementary Figure 1, the RPM for each gene, across both time-points and replicates, showing a
184 strong congruence between the two strains. Of the 132 conserved genes, 125 showed significant
185 differential expression in both strains. 119 of these 125 showed the same down- or up-regulated
186 patterns of significant differential expression from 5 hpi to 16 hpi (Figure 3c, early genes in blue, late
187 genes in red). The exceptions are D205R, CP80R, C315R, NP419L, F165R, and DP148R (MGF 360-
188 18R), encoding RNA polymerase subunits RPB5 and RPB10 (15), Transcription Factor IIB (TFIIB) (15),
189 DNA ligase (48), a putative signal peptide-containing protein, and a virulence factor (49),
190 respectively. The ASFV-TFIIB homolog (C315R) is classified as an early gene in GRG but not in BA71V,
191 in line with the predominantly early-expressed TBP (B263R), its predicted interaction partner. It is
192 worth noting however, that D205R, CP80R, and C315R are close to the threshold of significance, with
193 transcripts being detected at both 5 hpi and 16 hpi (Supplementary Table 1e).

194 Increased and pervasive transcription during late infection

195 During late infection of BA71V (10), we noted an increase in genome-wide mRNA abundance, as well
196 as an increasing number of TSSs and transcription termination sites, reminiscent of pervasive
197 transcription observed during late infection of Vaccinia virus (50). To quantify and compare the
198 global mRNA increase both in BA71V and GRG, we calculated the ratio of read coverage per
199 nucleotide, at 16 hpi versus 5 hpi (log2 transformed ratio of RPM), across the viral genome (Figure
200 4a, increase shown above- and decrease below the x-axis). This dramatic increase is due to the
201 overall increase of virus mRNAs present, which is visible in both strains (Figure 4b), with a ~2 fold
202 increase in GRG from 5 hpi to 16 hpi, versus ~8 fold in BA71V (Figure 4c).

203 This observation can at least in part be attributed to the larger number of viral genomes during late
204 infection, with increased levels of viral RNAP and associated factors available for transcription,
205 following viral protein synthesis. Viral DNA-binding proteins, such as histone-like A104R (51), may
206 remain associated with the genome originating from the virus particle in early infection. This could

207 suppress spurious transcription initiation, compared to freshly replicated nascent genomes that are
208 highly abundant in late infection. In order to test whether the increased mRNA levels correlated with
209 the increased number of viral genomes in the cell, we determined the viral genome copy number by
210 using quantitative PCR (qPCR against the p72 capsid gene sequence) using purified total DNA from
211 infected cells isolated at 0 hpi, 5 hpi and 16 hpi, and normalized values to the total amount of input
212 DNA. Using this approach, we observed genome copy levels that were consistent from 0 hpi to 5 hpi,
213 consistent with this being pre-DNA replication, followed by a substantial increase at 16 hpi, which
214 was more pronounced in BA71V infection (Figure 4d). This corresponded to a 15-fold increase in
215 GRG genome copy numbers from late, compared to early times post-infection of porcine
216 macrophages, and a 30-fold increase in BA71V during infection of Vero cells (Figure 4e). In summary,
217 the ASFV transcriptome changes both qualitatively and quantitatively as infection progresses, and
218 the increase of virus mRNAs during late infection is accompanied by the dramatic increase in viral
219 genome copies. Interestingly, the increase in viral transcripts and genome copies was less dramatic
220 in the virulent GRG strain.

221 Correcting the bias of temporal expression pattern

222 The standard methods of defining differential gene expression are well established in
223 transcriptomics using programs like DESeq2 (47). This is a very convenient and powerful tool which
224 captures the nuances of differential expression in complex organisms. However, virus transcription is
225 often characterised by more extreme changes, typically ranging from zero to millions of reads.
226 Furthermore, in both BA71V and GRG strains the genome-wide mRNA levels and total ASFV reads
227 increase over the infection time course (Figure 4 and Supplementary Table 1a). As a consequence,
228 such normalisation against the total mapped transcripts per sample (RPM) generates overestimated
229 relative expression values at 5 hpi, and understates those at 16 hpi (10). In order to validate the
230 early-late expression patterns derived from CAGE-seq, we carried out RT-PCR for selected viral
231 genes, as this signal is proportionate to the number of specific mRNAs regardless of the level of
232 other transcripts – with the minor caveat that it can pick up readthrough transcripts from upstream
233 genes. We tested differentially expressed conserved genes including GRG early- (MGF 505-7R, MGF
234 505-9R, NP419L), and D345L which showed stable relative expression values (RPM values in Figure
235 1e). All selected genes showed a consistently stronger RT-PCR signal during late infection in both
236 BA71V and GRG (Figure 5a-d). The exception is NP419L whose levels were largely unchanged, and
237 this is an example of how a gene whose transcript levels remain constant would be considered
238 downregulated, when almost all other mRNA levels increase (Figure 5b).

239 The standard normalisation of NGS reads against total mapped reads (RPM) is regularly used as it
240 enables a statistical comparison between samples and conditions, subject to experimental variations
241 (52). Keeping this in mind, we used an additional method of analysing the 'raw' read counts to
242 represent global ASFV transcript levels that are not skewed by the normalisation against total
243 mapped reads. Figure 5 shows a side-by-side comparison of RT-PCR results, and the CAGE-seq data
244 normalised (RPM) or expressed as raw counts, beneath each RT-PCR gel. Unlike CAGE-seq, RT-PCR
245 will detect transcripts originating from read-through of transcripts initiated from upstream TSS
246 including intra-ORF TSS (ioTSSs). To detect such 'contamination' we used multiple primer
247 combinations in upstream and downstream segments of the gene (Figure 5c, cyan and yellow
248 arrows) to capture and account for possible variations. Overall, our comparative analyses shows that
249 the normalised data (RPM) of early genes such as MGF 505-7R and 9R indeed skews and
250 overemphasises their early expression, while the raw counts are in better agreement with the mRNA
251 levels detected by RT-PCR. In contrast, late genes such as NP419L and D345L would be categorised
252 as late using all three quantification methods, in agreement with GRG CAGE-seq but not BA71V from
253 Figure 3c. We validated the expression pattern of the early GRG-specific gene MGF 360-12L (Figure
254 5e). While the RPM values indicated a very strong decrease in mRNA levels from early to late time
255 points, the decrease in raw counts was less pronounced and more congruent with the RT-PCR
256 analysis, showing a specific signal with nearly equal intensity during early and late infection. Lastly,
257 we used qRT-PCR to quantify C315R transcript levels, as this was close to the early vs late threshold,
258 (a log2fold change of 0 in Figure 3c), which showed again that qRT-PCR better agreed with the raw
259 counts.

260 An improved temporal classification of ASFV genes

261 Based on the considerations above, we prepared a revised classification of temporal gene expression
262 of the genes conserved between the two strains based on raw counts. The heatmap in Figure 6a
263 shows the mRNA levels at early and late infection stages of BA71V and GRG strains (all in duplicates)
264 with the genes clustered into five subcategories (1 to 5, Figure 6a) according to their early and late
265 expression pattern, which are shown in Figure 6b. Genes that are expressed at high or intermediate
266 levels during early infection but that also show high or intermediate mRNA levels during late
267 infection are classified as 'early' genes belonging to cluster-1 (8 genes, levels: high to high, H-H),
268 cluster-4 (33 genes, mid to mid, M-M) and cluster-5 (16 genes, low-mid to low-mid, LM-LM). Genes
269 with low or undetectable mRNA levels during early infection, which increase to intermediate or high
270 levels during late infection are classified as 'late' genes and belong to cluster-2 (15 genes, low to
271 high, L-H) and cluster-3 (60 genes, low to mid, L-M), respectively. Overall, the clustered heatmap

272 based on raw counts shows a similar but more emphasised pattern compared to the normalised
273 (RPM) data (compare Figure 6 and Supplementary Figure 1). Calculating the percentage of reads per
274 gene, which can be detected at 16 hpi compared to 5 hpi, reveals only a small number of genes have
275 most (≥70%) of their reads originating during early infection: 30 genes in the GRG strain and 5 genes
276 in the BA71V strain. For over half of the BA71V-GRG conserved genes, 90-100 % of reads can be
277 detected during late infection (Figure 6c). For all GRG genes, this generates a significant difference
278 between the raw counts per gene between time-points (Figure 6d).

279 Below we discuss specific examples of genes subcategorised in specific clusters. I73R is among the
280 top twenty most-expressed genes during both early and late infection according to the normalised
281 RPM values (Figure 2c and d) resides in cluster-1 (H-H) (Figure 6a). While I73R is expressed during
282 early infection, the mRNA levels remain high with >1/3 of all reads detected during late infection in
283 both strains when calculated as raw counts (34 % in GRG and 45 % in BA71V). This new analysis
284 firmly locates I73R into cluster-1 (H-H) and is classified confidently as early gene. Notably, our new
285 approach results in biologically meaningful subcategories of genes that are likely to be coregulated,
286 e. g. the eight key genes that encode the ASFV transcription system including RNAP subunits RPB1
287 (NP1450L), RPB2 (EP1242L), RPB3 (H359L), RPB5 (D205R), RPB7 (D339L) and RPB10 (CP80R), the
288 transcription initiation factor TBP (B263R) and the capping enzyme (NP868R) belong to cluster-4 (M-
289 M), and transcription factors TFIIS (I243L) and TFIIB (C315R) belong to cluster-5 (LM-LM). The overall
290 mRNA levels of cluster-4 and -5 genes are different, but remain largely unchanged during early and
291 late infection, consistent with the transcription machinery being required throughout infection. In
292 contrast, the mRNAs encoding the transcription initiation factors D6 (D1133L) and A7 (G1340L) are
293 only present at low levels during early- but increase during late infection and thus belong to cluster-
294 3 (L-M), classifying them as late genes. This is meaningful since the heterodimeric D6-A7 factor is
295 packaged into viral particles (7), presumably during the late stage of the infection cycle. The mRNAs
296 of the major capsid protein p72 (B646L) and the histone-like-protein A104R (51,53) follow a similar
297 late pattern but are present at even higher levels during late infection and therefore belong to
298 cluster-2 (L-H).

299 Architecture of ASFV promoter motifs

300 In order to characterise early promoter motifs (EPM) in the GRG strain, we extracted sequences 35
301 bp upstream of all early gene TSSs and carried out multiple sequence alignments. As expected, this
302 region shows a conserved sequence signature in good agreement with our bioinformatics analyses
303 of EPMs in the BA71V strain, including the correct distance between the EPM and the TSS (9-10 nt
304 from the EPM 3' end) and the 'TA' motif characteristic of the early gene Initiator (Inr) element

305 (Figure 7a) (10). A motif search using MEME (54) identified a core (c)EPM motif with the sequence
306 5'-AAAATTGAAT-3' (Figure 7b), within the longer EPM. The cEPM is highly conserved and is present
307 in almost all promoters controlling genes belonging to cluster-1, -4 and -5 (Supplementary Table 3).
308 A MEME analysis of sequences 35 bp upstream of late genes (Figure 7c), provided a 17-bp AT-rich
309 core late promoter motif (cLPM, Figure 7d), however, this could only be detected in 46 of the late
310 promoters.

311 In an attempt to improve the promoter motif analyses and deconvolute putative sequence elements
312 further, we probed the promoter sequence context of the five clusters (clusters 1-5 in Figure 7e-i,
313 respectively) of temporally expressed genes with MEME (Supplementary Table 3). The early gene
314 promoters of clusters-1 (H-H), -4 (M-M) and -5 (LM-LM) are each associated with different
315 expression levels, and all of them contain the cEPM located 15-16 nt upstream of the TSS with two
316 exceptions that are characterized by relatively low mRNA levels (Figure 7k). Interestingly, cluster-2
317 (L-H) promoters are characterized by a conserved motif with significant similarity to eukaryotic
318 TATA-box promoter element that binds the TBP-containing TFIID transcription initiation factor
319 (Figure 7f highlighted with red bracket, detected via Tomtom (55) analysis of the MEME motif
320 output). Cluster-3 (L-M) promoters contain a long motif akin to the cLPM, derived from searching all
321 late gene promoter sequences, and which is similar to the LPM identified in BA71V (Figure 7d and g,
322 green bracket). All motifs described in the cluster analysis above could be detected with statistically
323 significance (p-value < 0.05) via MEME, in every gene in each respective cluster with only two
324 exceptions: MGF 110−3L from cluster-1, and MGF 360-19R from cluster-4, for the latter see details
325 below.

326 Updating Genome Annotations using Transcriptomics Data

327 TSS-annotation provides a useful tool for re-annotating predicted ORFs in genomes like ASFV (10)
328 where many of the gene products have not been fully characterized and usually rely on prediction
329 from genome sequence alone. We have provided the updated ORF map of the GRG genome in GFF
330 format (Supplementary Table 1f). This analysis identified an MGF 360-19R ortholog (Figure 8),
331 demonstrating how transcriptomics enhances automated annotation of ASFV genomes by predicting
332 ORFs from TSSs. The MGF 360-19R was included in subsequent DESeq2 analysis showing it was not
333 highly nor significantly differentially expressed (Supplementary Table 1e). Another important feature
334 is the identification of intra-ORF TSSs (ioTSSs) within MGF 360-19R that potentially direct the
335 synthesis of N-terminally truncated protein variants expressed either during early or late infection.
336 The presence of EPM and LPM promoter motifs lends further credence to the ioTSSs (Figure 8).
337 Similar truncation variants were previously reported for I243L and I226R (56) and in BA71V (10). In

338 addition, we detected multiple TSSs within MGF 360-19R encoding very short putative novel ORFs
339 (nORF) 5, 7 or 12 aa residues long; since these ioTSSs were present in both early and late infection
340 they are not all likely to be due to pervasive transcription during late infection.

341 We investigated the occurrence of ioTSS genome wide and uncovered many TSSs with ORFs
342 downstream that were not annotated in the GRG genome (Supplementary Table 2a). These ORFs
343 could be divided into sub-categories: in-frame truncation variants (Supplementary Table 2b, akin to
344 MGF 360-19R in Figure 8), nORFs (Supplementary Table 2c), and simply mis-annotated ORFs. All
345 updated annotations are found in Supplementary Table 1f. Putative truncation variants generated
346 from ioTSSs were predominantly identified during late infection, suggesting these could be a by-
347 product of pervasive transcription. Therefore, those detected early or throughout infection are
348 perhaps more interesting, they span a variety of protein functional groups, and many gene-products
349 are entirely uncharacterised (Figure 9a). The truncation variants additionally showed a size variation
350 of 5'-UTRs between the ioTSSs and downstream start codon (Figure 9b). An example of a mis-
351 annotation would be CP204L (Phosphoprotein p30, Figure 9c) gene that is predicted to be 201
352 residues long. The TSS determined by CAGE-seq and validated by Rapid Amplification of cDNA Ends
353 (5'-RACE) is located downstream of the annotated start codon; based on our results we reannotated
354 the start codon of CP204L which results in a shorter ORF of 193 amino acids (Figure 9c).

355 Our GRG TSS map led to the discovery of many short nORFs, which are often overlooked in
356 automated ORF annotations due to a minimum size, e. g. 60 residues in the original BA71V
357 annotation (15). Some short ORFs have been predicted for the GRG genome including those labeled
358 'ASFV_G_ACD' in the Georgia 2007/1 genome annotation (19). However, their expression was not
359 initially supported by experimental evidence, though we have now demonstrated their expression
360 via CAGE-seq (Figure 2b, Supplementary Table 1e). We have now identified TSSs for most of these
361 short ORFs, indicating at minimum they are transcribed. As described above, we noted that TSSs
362 were found throughout the genome in intergenic regions in addition to those identified upstream of
363 the 190 annotated GRG ORFs (including MGF 360-19R, Supplementary Table 2c). Our systematic,
364 genome-wide approach identified 175 novel putative short ORFs. BLASTP (57) alignments showed
365 that 13 were homologous to ORFs predicted in other strains, including DP146L and pNG4 from
366 BA71V . We validated the TSSs for these candidates using 5'-RACE, which demonstrates the presence
367 of these mRNAs and their associated TSSs at both time-points (Figure 9d and e, respectively),
368 compared to our CAGE-seq data (Figure 9f and g, respectively).

369 ## Putative single-SH2 domain protein encoding genes in MGF 100

370 Our understanding of the ASFV genome is hampered by the large number of genes with unknown
371 functions. We approached this problem by searching for conserved domains of uncharacterised MGF
372 members *in silico*. MGF 100 genes form the smallest multigene family and include three short (100–
373 150 aa) paralogs located at both genome ends (right, R and left, L): 1R, 1L (MGF_100-2L or DP141L in
374 BA71V), and 3L (DP146L in BA71V). We predicted the two highly similar GRG ORFs I7L and I8L (51%
375 sequence identity) to belong to the MGF 100 family (Figure 10a), as designated in the Malawi
376 LIL20/1 strain (58). Both I7L and I8L show similar overall transcript levels to the annotated MGF 100
377 members -1L and 1R, though newly annotated MGF 100-3L (nORF_180573) was expressed at much
378 higher levels. I7L and I8L are both early genes like MGF 100-3L, while MGF 100-1L and 1R are
379 expressed late and not significantly changing, respectively (Supplementary Table 1e). Several lines of
380 evidence suggest that I7L and I8L play an role during infection. I7L and I8L are expressed early and at
381 high levels, their deletion along with L9R, L10L, and L11L ORFs reduces virulence in swine (59), and
382 their loss is associated with the adaptation of the GRG2007/1 strain to tissue culture infection (60).
383 To gain insight into the function of MGF family members including I7L and I8L, we generated
384 computational homology models of MGF 100-1L -1R, I7L and I8L using Phyre2 (61) (Figure 10b). The
385 structures selected by the algorithm for the modeling of MGF 100 proteins, included suppressor of
386 cytokine signalling proteins 1 and -2, and the PI3-kinase subunit alpha, all of which are characterized
387 by Src Homology 2 (SH2) domains (Figure 10b and Supplementary Table 2d). Canonical SH2 domains
388 bind to phosphorylated Tyrosine residues and are an integral part of signalling cascades involved in
389 the immune response (62). HHpred searches (63) predicted that indeed all MGF 100 members in
390 BA71V and GRG include SH2 domains (Figure 10c).

391 ## The response of the porcine macrophage transcriptome to ASFV infection

392 In order to evaluate the impact of ASFV on the gene expression of the host cell, we analysed
393 transcriptomic changes of infected porcine macrophages using the CAGE-seq data from the control
394 (uninfected cells), 5 hpi, and 16 hpi. We annotated 9,384 macrophage-expressed protein-coding
395 genes with CAGE-defined TSSs (Supplementary Table 4). Although primary macrophages are known
396 to vary largely in their transcription profile, the CAGE-seq reads were highly similar between RNA
397 samples obtained from macrophages from two different animals in this study (Spearman's
398 correlation coefficients ≥ 0.77).

399 As TSSs are not well annotated for the swine genome, we annotated them *de novo* using our CAGE-
400 seq data with the RECLU pipeline. 37,159 peaks could be identified, out of which around half
401 (18,575) matched unique CAGE-derived peaks annotated in Robert et al. (64) i.e. they were located

402 closer than 100 nt to the previously described peaks. Mapping CAGE-seq peaks to annotated swine
403 protein-coding genes led to identification of TSSs for 9,384 macrophage-expressed protein-coding
404 genes (Supplementary Table 4). The remaining 11,904 swine protein-coding genes did not have
405 assigned TSSs, and therefore their expression levels were not assessed. The majority of genes were
406 assigned with multiple TSSs, and these TSS-assigned genes, corresponded to many critical functional
407 macrophage markers, including genes encoding 56 cytokines and chemokines (including CXCL2,
408 PPBP, CXCL8 and CXCL5 as the most highly expressed), ten S100 calcium binding proteins (S100A12,
409 S100A8, and S100A9 in the top expressed genes), as well as interferon and TNF receptors (IFNGR1,
410 IFNGR2, IFNAR1, IFNAR2, IFNLR1, TNFRSF10B, TNFRSF1B, TNFRSF1A, etc.), and typical M1/M2
411 marker genes such as TNF, ARG1, CCL24, and NOS2 (Supplementary Table 5

412 The 9,384 genes with annotated promoters were subjected to differential expression analysis using
413 DESeq2 to compare the 5 and 16 hour infected cell time points with control non-infected cells (c, 5
414 and 16) in a pairwise manner i.e. between each condition. Expression of only 25 host genes was
415 significantly deregulated between the control and 5 hpi, compared to 652 genes between 5 hpi and
416 16 hpi, and 1325 genes between mock-infected and 16 hpi (at FDR of 0.05). Based on the pairwise
417 comparisons, we could distinguish major response profiles of the host genes. Late response genes,
418 whose expression was significantly deregulated both between the uninfected control and 16 hpi and
419 5 and 16 hpi, and early response genes, whose expression was significantly deregulated between the
420 control and 5 hpi, but not 5-16 hpi (Figure 11a). The latter category included only 20 genes, whereas
421 more than 500 genes showed the late differentially regulated response: 344 genes were up-
422 regulated, and 180 genes were down-regulated. The majority of the > 9000 genes analysed
423 therefore were not differentially regulated. Comparison of differences between expression levels in
424 the different samples indicate that macrophage differentially expressed transcription programs
425 change mostly between 5 and 16 hpi (Figure 11b and c). The upregulated late response genes with
426 highest expression levels included several S100 calcium binding proteins. In contrast, expression of
427 important cytokines (including CCL24, CXCL2, CXCL5 and CXCL8) significantly decreased from 5 hpi to
428 16 hpi (Figure 11d).

429 To investigate the transcriptional response pathways and shed light on possible transcription factors
430 involved in the macrophage response to ASFV infection, we searched for DNA motifs enriched in
431 promoters of the four categories of deregulated genes in Figure 11a. Both late response promoter
432 sets were significantly enriched with motifs, some of which contained sub-motifs known to be
433 recognised by human transcription factors (Supplementary Figure 2). The highest-scored motif found
434 in promoters of upregulated genes contained a sub-motif recognised by a family of human

435 interferon regulatory factors (IRF9, IRF8 and IRF8, (Supplementary Figure 2a) that play essential roles
436 in the anti-viral response. Interestingly, both upregulated and downregulated promoters
437 (Supplementary Figure 2b and c, respectively) were enriched with extended RELA/p65 motifs. p65 is
438 a Rel-like domain-containing subunit of the NF-kappa-B complex, regulated by I-kappa-B, whose
439 analog is encoded by ASFV. This pathway being a known target for ASFV in controlling host
440 transcription (65–68).

441 To understand functional changes in the macrophage transcriptome, we also performed gene set
442 enrichment analysis using annotations of human homologs. The top enriched functional annotations
443 in the upregulated late response genes include glycoproteins and disulfide bonds, transmembrane
444 proteins, innate immunity, as well as positive regulation of inflammatory response (Figure 11e). In
445 contrast, sterol metabolism, rRNA processing, cytokines, TNF signalling pathway, inflammatory
446 response as well as innate immunity were the top enriched functional clusters among the
447 downregulated late response genes. Interestingly, the genes associated with innate immunity
448 appear overrepresented in both up- and downregulated gene subsets, yet cytokines are 8-fold
449 enriched only in the downregulated genes). The mRNA levels of genes of interest were additionally
450 verified using RT-PCR (Figure 11f).

451 Protein expression of selected genes.

452 In order to determine whether the regulation exerted by GRG on host transcription of
453 immunomodulatory genes could also translate to protein levels, we selected representative proteins
454 whose genes showed significant changes. ISG15 expression, part of the antiviral response genes of
455 the type I IFN stimulation pathway, was measured with Western blot (Figure 12a), with ASFV
456 infection being monitored via P30 levels (Figure 12b). Cytokines released from infected PAMS were
457 quantified using ELISA tests for pig cytokines, TNF-α, CXCL8 and CCL2 (Figure 12c, d and e,
458 respectively). As shown in Figure 12, the release/expression for all the tested proteins during GRG
459 infection were similar or decreased in comparison to the control uninfected cells at both 5 hpi and
460 16 hpi, while the production of viral protein P30 increased, confirming an effective viral infection.

461 Discussion [3,009 words]

462 In order to shed light on the gene expression determinants for ASF virulence, we focussed our
463 analyses on the similarities and differences in gene expression between a highly virulent Georgia
464 2007/1 isolate and a nonvirulent, lab-adapted strain BA71V. Previous annotation identified 125 ASFV
465 ORFs that are conserved between all ASFV strain genomes irrespective of their virulence (16). They
466 represent a 'core' set of genes required for the virus to produce infectious progeny and include gene

467 products like those involved in virus genome replication, virion assembly, RNA transcription and
468 modification. These genes are located in the central region of the genome (Figure 1a). Besides such
469 essential genes, about one third are non-essential for replication, but have roles in evading host
470 defence pathways. Some genes are conserved between isolates, but not necessarily essential core
471 genes, for example apoptosis inhibitors: Bcl-2 family member A179L and IAP family member A224L
472 (69). Other non-essential genes, especially MGF members, vary in number between isolates. Our
473 transcriptomic analysis captured TSS signals from 119 genes both shared between the BA71V and
474 GRG genomes, which also matched expression patterns during early and late infection, according to
475 CAGE-seq (Figure 3, Figure 4a-c). Outliers include DP148R, which is unsurprising, given its promoter
476 region is deleted in BA71V, and its coding region is interrupted by a frame shift mutation, therefore
477 functional protein expression unlikely. DP148R is a non-essential, early-expressed virulence factor in
478 the Benin 97/1 strain (49) – consistent with our GRG data. Many additional GRG genes, lost from
479 BA71V are MGFs, which are mostly upregulated during early infection and located at the ends of the
480 linear genome (Figure 1a). MGFs have evolved on the virus genome by gene duplication, and do not
481 share significant similarity to other proteins, though some conserved domains, including ankyrin
482 repeats, are present in some MGF 360 and 505 family members (17,19).

483 Using advanced sequence searches and computational homology modelling we predict the members
484 of the MGF 100 family to encode SH2 domains, including I7L and I8L. Although SH2 domains are
485 primarily specific to eukaryotes, rare cases of horizontally transferred SH2 domains found in viruses,
486 are implicated in hijacking host cell pTyr signalling (70). A large family of 'super-binding' SH2
487 domains were discovered in Legionella. Its members, including single SH2 domain-proteins are likely
488 effector proteins during infection (71). We also identified a further MGF 100 member in the GRG
489 genome as one of our nORFs, a partial 100-residue copy of DP146L (MGF 100-3L) (Supplementary
490 Table 2c). Unlike its annotated MGF 100-1L and MGF 100-1R cousins it was downregulated from 5
491 hpi to 16 hpi (Supplementary Table 1e). Together with I7L and I8L, GRG encodes a total of 5 MGF
492 100 genes (Figure 10a). Interestingly, loss of MGF 100 members was observed during the process of
493 adapting a virulent Georgia strain to grow in cultured cell lines (60). Deletion of MGF 100-1R, from a
494 virulent genotype II Chinese strain (72) or of l8L from Georgia 2010 was shown not to reduce
495 virulence of the virus in pigs or reduce virus replication in porcine macrophages (73). However,
496 simultaneous deletion of genes l7L, l8L, l9L, l10L and l11L from a Chinese virulent isolate reduced
497 virulence and surviving pigs were protected against challenge (59). In summary, although deletion of
498 some individual MGF 100 genes does not lead to attenuation, deletion of l7L and l8L, in combination
499 with l9L, l10L, and l11L did have an impact.

500 The Georgia 2007/1 genome was recently re-sequenced which identified a small number of genome
501 changes affecting mapped ORFs and identified new ORFs (18). Adjacent to the covalently cross-
502 linked genome termini, the BA71V genome contains terminal inverted repeats of >2 kbp, in which
503 two short ORFs were identified (DP93R, DP86L). These were not included in previous GRG sequence
504 annotations, however our nORFs included a 55-residue homolog of DP96R, which was a late, but not
505 highly expressed gene. These are yet further examples of how transcriptomics aid in improving ASFV
506 genome annotation. Functional data is available for only a few of proteins coded by ORFs not
507 conserved between BA71V and GRG. This includes the p22 protein (KP177R), which is expressed on
508 the cell membrane during early infection, and also incorporated into the virus particle inner
509 envelope. The function of the KP177R-like GRG gene l10L has not been studied, but may provide an
510 antigenically divergent variant of P22, enabling evasion of the host immune response (19). We found
511 KP177R was highly expressed at 16 hpi, while l10L was also expressed late, but at much lower levels.
512 Their function is unknown, though the presence of an SH2 domain indicates possible roles in
513 signalling pathways (7,19,74).

514 MGF 110 members are among the highest expressed genes during early infection both in GRG (this
515 study), and in BA71V (10), suggesting high importance during infection, at least in porcine
516 macrophages and Vero cells, respectively. However, MGF 110 remains poorly characterised, and 13
517 orthologues were identified thus far, with numbers present varying between isolates (30). MGF 110
518 proteins possess cysteine-rich motifs, optimal for an oxidizing environment as found in the
519 endoplasmic reticulum (ER) lumen or outside the cell, and MGF 110-4L (XP124L) contains a KDEL
520 signal for retaining the protein in the ER (75). Since highly virulent isolates have few copies of these
521 genes (for example, only 5 in the Benin 97/1 genome), it was assumed they are not importance for
522 virulence in pigs (17), but their high expression warrant further investigation, which has recently
523 begun in the form of deletion mutants. For example, deletion of MGF 110-9L from a Chinese
524 genotype II virulent strain, reduced virulence (35), whereas deletion of MGF 110-1L from Georgia
525 2010 (76) did not substantially affect virulence.

526 There is however, good evidence that MGF 360 and 505 carry out important roles in evading the
527 host type I interferon (IFN) response - the main host antiviral defence pathway (37). Evidence for the
528 role of MGF 360 and 505 genes in virulence was obtained from deletions in tissue-culture adapted
529 and field attenuated isolates, as well as targeted gene deletions This correlated with induction of the
530 type I interferon response, which itself is inhibited in macrophages infected with virulent ASFV
531 isolates (32,38,39). Deletions of these MGF 360, and 505 genes also correlated with an increased
532 sensitivity of ASFV replication, to pre-treatment of the macrophage cells with type I IFN (40). Thus,

533 the MGF 360 and 505 genes have roles in inhibiting type I IFN induction and increasing sensitivity to
534 type I IFN. However, it remains unknown if these MGF 360 and MGF 505 genes act synergistically or
535 if some have a more important role than others type I IFN suppression. Our DESeq2 analysis did
536 show that members of both these families showed very similar patterns of early expression (Figure 2
537 and Figure 3), conserved cEPM-containing promoters, and almost exclusive presence in clusters-1
538 (H-H), -4 (M-M), and -5 (LM-LM) (Figure 6 and Figure 7), consistent with ASFV prioritising inhibition
539 of the host immune response during early infection.

540 An interesting pattern which emerged during our CAGE-seq analysis was the clear prevalence of
541 ioTSSs within ORFs, especially in MGFs (Figure 8 and Figure 9). However, it is not clear whether
542 subsequent in-frame truncation variants generate stable proteins, nor what their function could be.
543 Perhaps even more interesting was the discovery of 176 nORFs (including MGF 360-19R), with clear
544 TSSs according to CAGE-seq, highlighting the power of transcriptomics to better annotate sequenced
545 genomes. We were able to detect previously unannotated genes from other strains, and partial
546 duplications of genes already encoded in GRG (Supplementary Table 2).

547 The increase in transcription across the ASFV genome during late infection (10), appears ubiquitous.
548 At least 50 genes have previously been investigated in single gene expression studies using Northern
549 blot or primer extension (for review see references (10,77). Transcripts from over two thirds of these
550 genes were detected during late infection, and a quarter had transcripts detected during both early
551 and late infection. Therefore, clear evidence using several techniques now support this increase in
552 ASFV transcripts at late times post-infection. It is not entirely clear whether it is due to pervasive
553 transcription, high mRNA stability or a combination of factors. However, there is a correlated
554 increase in viral genome copies, potentially available as templates for pervasive transcription. The
555 increase in genome copies is more pronounced in BA71V compared to GRG, which likewise is
556 reflected in the increase in transcripts during late infection (Figure 4).

557 Our transcriptomic analysis of the porcine macrophage host revealed 522 genes whose expression
558 patterns significantly changed between 5 and 16 hrs post-infection (Figure 11a) and only 20 genes
559 were found to change between the control cells and those infected for 5 hpi. In aggregate, this
560 reflects a relatively slow host response to ASFV infection following expression of early ASFV genes.
561 We observed mild downregulation of some genes e.g. ACTB coding for ß-actin, eIF4A, and eIF4E
562 (Supplementary Table 5), resembling patterns previously shown by RT-qPCR (78). The macrophage
563 transcriptome mainly shuts down immunomodulation between 5 hpi to 16 hpi post-infection;
564 cytokines appeared highly expressed at 5 hpi, but downregulated from 5 hpi to 16 hpi. Of the 54

565 cytokine genes we detected, expression of thirteen was decreased: four interleukin genes (IL1A,
566 IL1B, IL19, IL27), four pro-inflammatory chemokines (CCL24, CXCL2, CXCL5, CXCL8), and tumor
567 necrosis factor (TNF) genes. Since inflammatory responses serve as the first line of host defense
568 against viral infections, viruses have developed ways to neutralise host pro-inflammatory pathways.
569 ASFV encodes a structural analog of IκB, A238L, which was proposed to act as a molecular off-switch
570 for NFκB-targeted pro-inflammatory cytokines (67). In our study, A238L is one of the most expressed
571 ASFV genes at 5 hpi, but significantly downregulated afterwards (Figure 2c). Accordingly, swine
572 homologs of human NFκB target genes were significantly over-represented (3.8 fold) among
573 downregulated macrophage genes (Fisher's exact p-value < 1e-5, based on human NFκB target genes
574 from https://www.bu.edu/nf-kb/gene-resources/target-genes/). Downregulated genes include
575 interleukins 1A, 1B, and 8, and 27 (IL1A, IL1B, CXCL8, IL27), TNF, as well as a target for common
576 nonsteroidal anti-inflammatory drugs, prostaglandin-endoperoxide synthase 2 (PTGS2 or COX-2)
577 (Supplementary Figure 2). Interestingly, promoters of both up- and downregulated genes contained
578 a motif with the sequence preferentially recognised by the human p65-NFκB complex (79).
579 Expression of TNF, a well-known marker gene for acute immune reaction and M1 polarisation, was
580 recorded at a high level in control samples and at 5 hpi, but significantly dropped at 16 hpi. It has
581 been already shown that ASFV inhibits transcription of TNF and other proinflammatory cytokines
582 (67). On the other hand, the downregulation of TNF stands in contrast to previous results from ASFV-
583 E75 strain-infected macrophages in vitro, where TNF expression increased significantly after 6 hpi
584 (80). Therefore, the different time courses of TNF expression induced by the moderately virulent E75
585 and more virulent Georgia strain may reflect different macrophage activation programs (81).

586 We investigated if the modulation of transcription we observed by CAGE-seq during GRG infection of
587 PAMS was also observed at the protein level. We analysed the secretion or expression of different
588 immunomediators (cytokines CCL2, CXCL8, TNF-α and interferon stimulated gene ISG15) at different
589 times following infection of PAMS. We confirmed that that the infection did not lead to an increase
590 of these mediators at either 5h or 16h infection. Secretion or expression of these proteins were
591 similar or slightly decreased in infected cells in comparison to control non-infected cells. The results
592 indicated that the control by virulent Georgia 2007/1 of host cell responses to infection we observed
593 at the transcription level can lead to a control also at the level of the protein production.
594 Interestingly, CCL2 transcription was somewhat upregulated at late infection (Supplementary Table
595 5), whereas its protein release to the supernatant was decreased (Figure 12e). ASFV has been shown
596 to prioritize expression of its encoded proteins by sequestering components of the host translation
597 machinery to viral factories (82). The levels or functions of host proteins may also be modulated by

598 targeting for post-translational modification or degradation (82–84). Therefore, in addition to
599 control at the transcriptional level ASFV may modulate the production of immunomodulatory host
600 proteins at a later step, as seems to occur for CCL2, a known chemoattractant for myeloid and
601 lymphoid cells (85), that could be an important target for regulation by ASFV.

602 Four S100 family members are among the host genes that are upregulated after 5 hpi (Figure 11b)
603 including S100A8, S100A11, S100A12, and S100A13. S100A8 and S100A12 are among the most
604 highly expressed genes on average throughout infection. S100 proteins are calcium-binding cytosolic
605 proteins that are released and serve as a danger signal, and stimulate inflammation (86). Once
606 released from the cell, S100A12 and S100A8 function as endogenous agonists to bind TLR4 and
607 induce apoptosis and autophagy in various cell types (86). S100A8 and S100A9 were also found in
608 the RNA-seq whole blood study as the top upregulated upon infection of the pigs with Georgia
609 2007/1, but not of a low pathogenic ASFV isolate OURT 88/3 (43).

610 Previous studies described global swine transcriptome changes upon ASFV infection using short read
611 sequencing (Illumina): including the RNA-seq described above (43) and a microarray study of primary
612 swine macrophage cell cultures infected with the GRG strain, at six time points post-infection (42).
613 Although these varied in designs and selected methods, results of these works both give some
614 indication into the main host immune responses and ways how ASFV could evade them. The latter
615 microarray study indicated similar suppression of inflammatory response after 16 hpi as we
616 observed in this study, with expression of many cytokines down-regulated relative to non-infected
617 macrophages (42). More-recently, there have been several transcriptomic studies using classical
618 RNA-seq of ASFV infections from Chinese isolates (44–46). Fan et al (44) investigated the
619 transcriptomic and proteomic response within tissues of pigs following ASFV infection and death,
620 though this was not directly comparable to our own analysis in PAMs, due to their observations
621 being of a far later infection stage (post-mortem) than our 16 hrs time-point. The two most-
622 comparable studies to ours were carried out on a Chinese genotype II pathogenic strain during
623 infection of PAMs. Ju et al. (45) investigated 6, 12 and 24 hpi, while Yang et al. (46) investigated 12,
624 24, and 36 hpi. However, comparison of the overlapping time points of 12 hpi and 24 hpi did not
625 yield similar host gene expression changes, possibly due to variation among primary macrophages or
626 due to the low MOI of 1 used in both studies. In summary, these differences highlight that our
627 understanding of the host-virus relationship during ASFV infection is still not well understood, and
628 further work is needed to understand why such substantial variation in host gene expression can
629 arise.

630 A further important note, is that all of the studies described above are using classical RNA-seq-based
631 methods, the nucleotide resolution of which, is not sufficient to investigate differential expression of
632 both the virus and host simultaneously. Investigating the viral transcriptome is especially difficult in
633 a compact genome like that of ASFV, where transcription read-through can undermine results from
634 classical RNA-sequencing techniques (10,87). A recent investigation into ASFV RNA transcripts using
635 long-read based Oxford Nanopore Technologies (ONT) – provides fascinating insight into their length
636 and read-through heterogeneity. This new method highlighted how misleading short read
637 sequencing with classical RNA-seq can be when quantifying ASFV gene expression, due to the
638 abundance of readthrough occurring in ASFV, generating transcripts covering multiple viral ORFs.
639 This study did however, unfortunately lack the read coverage for in-depth analysis of host transcripts
640 alongside that of viral transcripts (88,89).

641 Here we have demonstrated that CAGE-seq is an exceptionally powerful tool for quantifying relative
642 expression of viral genes across the ASFV genome, as well as making direct comparison between
643 strains for expression of shared genes, and further highlighting the importance of highly-expressed
644 but still functionally uncharacterised viral genes. CAGE-seq conveniently circumvents the issue in
645 compact viral genomes like those of ASFV and VACV, of transcripts reading through into downstream
646 genes which cannot be distinguished from classical short-read RNA-seq (10,43,90). Furthermore, it
647 enables us to effectively annotate genome-wide, the 5’ ends of capped viral transcripts, and thus
648 TSSs of viral genes, and subsequently their temporal promoters. This 5' end resolution in ASFV is still
649 not achievable via ONT long read sequencing (88,89). We have now expanded on promoter motifs
650 we previously described (Figure 7), to identify 5 clusters of genes (Figure 6), with distinct patterns of
651 expression. Three of these clusters (-1: high to high levels, -4: mid to mid, and -5 low-mid to low-
652 mid) have slightly differing promoters, with a highly conserved core EPM. This is akin to the early
653 gene promoter of VACV (87) for VETF recognition and early gene transcription initiation (13,91,92).
654 We have found late genes can be categorised into two types that either increase from low to
655 extremely high expression levels (e. g. p72-encoding B646L) in cluster-2, or from low to medium
656 expression levels in cluster 3 (e. g VETF-encoding genes). The promoters of these genes show
657 resemblance to the eukaryotic TATA-box (93) or the BA71V LPM (10), respectively. Our analysis
658 additionally shows the potential for a variety of non-pTSSs: alternative ones used for different times
659 in infection, ioTSSs which could generate in-frame truncation variants of ORFs, sense or antisense
660 transcripts relative to annotated ORFs, and finally TSSs generating nORFs, which predominantly have
661 no known homologs.

662 In summary, it is becoming increasingly clear that the transcriptomic landscape of ASFV and its host
663 during infection is far more complex than originally anticipated. Much of this raises further questions
664 about the basal mechanisms underlying ASFV transcription and how it is regulated over the infection
665 time course. Which subsets of initiation factors enable the RNAPs to recognise early and late
666 promoters? Does ASFV include intermediate genes, and what factors enables their expression? What
667 is the molecular basis of the pervasive transcription during late infection? The field of ASFV
668 transcription has been understudied and underappreciated and considering the severe threat that
669 ASF poses for the global food system and -food security, we now need to step up and focus our
670 attention and resources to study the fundamental biology of ASFV to develop effective antiviral
671 drugs and vaccines.

672 Methodology [2871 words]

673 GRG-Infection of Macrophages and RNA-extraction

674 Primary porcine alveolar macrophage cells were collected from two animals following approval by
675 the local Animal Welfare and Ethical Review Board at The Pirbright Institute. Cells were seeded in 6-
676 well plates ($2x10^6$ cells/well) with RPMI medium (with GlutaMAX), supplemented with 10% Pig
677 serum and 100 IU/ml penicillin, 100 µg/ml streptomycin. They were infected as 2 replicate wells for
678 5 hpi or 16 hpi with a multiplicity of infection (MOI) of 5 of the ASFV Georgia 2007/1 strain, while
679 uninfected cells were seeded in parallel as a control (mock-infection). Total RNA was extracted
680 according to manufacturer's instructions for extraction with Trizol Lysis Reagent (Thermo Fisher
681 Scientific and the subsequent RNAs were resuspended in 50µl RNase-free water and DNase-treated
682 (Turbo DNAfree kit, Invitrogen). RNA quality was assessed via Bioanalyzer (Agilent 2100). 5 µg of
683 each sample was ethanol precipitated before sending to CAGE-seq (Kabushiki Kaisha DNAFORM,
684 Japan). Samples were named as follows: uninfected cells or 'mock' (C1-ctrl and C2-ctrl), at 5 hpi post-
685 infection (samples G1-5h and G2-5h), and at 16 hpi post-infection (G3-16h and G4-16h).

686 CAGE-sequencing and Mapping to GRG and *Sus scrofa* Genomes

687 Library preparation and CAGE-sequencing of RNA samples was carried out by CAGE-seq (Kabushiki
688 Kaisha DNAFORM, Japan). Library preparation produced single-end indexed cDNA libraries for
689 sequencing: in brief, this included reverse transcription with random primers, oxidation and
690 biotinylation of 5' mRNA cap, followed by RNase ONE treatment removing RNA not protected in a
691 cDNA-RNA hybrid. Two rounds of cap-trapping using Streptavidin beads, washed away uncapped
692 RNA-cDNA hybrids. Next, RNase ONE and RNase H treatment degraded any remaining RNA, and
693 cDNA strands were subsequently released from the Streptavidin beads and quality assessed via

694 Bioanalyzer. Single strand index linker and 3' linker was ligated to released cDNA strands, and primer
695 containing Illumina Sequencer Priming site was used for second strand synthesis. Samples were
696 sequenced using the Illumina NextSeq 500 platform producing 76 bp reads. FastQC (94) analysis was
697 carried out on all FASTQ files at Kabushiki Kaisha DNAFORM and CAGE-seq reads showed consistent
698 read quality across their read-length, therefore, were mapped in their entirety to the GRG genome
699 (FR682468.1) in our work using Bowtie2 (95), and *Sus scrofa* (GCF_000003025.6) genome with
700 HISAT2 (95,96) by Kabushiki Kaisha DNAFORM.

701 Transcription Start Site-mapping Across Viral GRG Genome

702 CAGE-seq mapped sample BAM files were converted to BigWig (BW) format with BEDtools (97)
703 genomecov, to produce per-strand BW files of 5' read ends. Stranded BW files were input for TSS-
704 prediction in RStudio (98) with Bioconductor (99) package CAGEfightR (100). Genomic feature
705 locations were imported as a TxDb object from FR682468.1 genome gene feature file (GFF3).
706 CAGEfightR was used to quantify the CAGE reads mapping at base pair resolution to the GRG
707 genome - at CAGE TSSs, separately for the 5 hpi and 16 hpi replicates. TSS values were normalized by
708 tags-per-million for each sample, pooled, and only TSSs supported by presence in both replicates
709 were kept. TSSs were assigned to clusters, if within 25 bp of one another, filtering out pooled, RPM-
710 normalized TSS counts below 25 bp for 5 hpi samples, or 50 bp for 16 hpi, and assigned a 'thick'
711 value as the highest TSS peak within that cluster. A higher cut-off for 16 hpi was used to minimise
712 the extra noise of pervasive transcription observed during late infection (10). TSS clusters were
713 assigned to annotated FR682468.1 ORFs using BEDtools intersect, if its highest point ('thick' region)
714 was located within 500 bp upstream of an ORF, 'CDS' if within the ORF, 'NA' if no annotated ORF was
715 within these regions. Multiple TSSs located within 500 bp of ORFs were split into subsets: 'Primary'
716 cluster subset contained either the highest scoring CAGEfightR cluster or the highest scoring
717 manually-annotated peak (when manual ORF corrections necessary), and the highest peak
718 coordinate was defined as the primary TSS (pTSS) for an ORF. Further clusters associated with these
719 ORFs were classified as 'non-primary', with their highest peak as a non-primary TSS (npTSS). If the
720 strongest TSS location was intra-ORF, without any TSSs located upstream of the ORF, then the ORF
721 was manually re-defined as starting from the next ATG downstream.

722 DESeq2 Differential Expression Analysis of GRG Genes

723 For analysing differential expression with the CAGE-seq dataset, a GFF was created with BEDtools
724 extending from the pTSS coordinate, 25 bp upstream and 75 bp downstream, however, in cases of
725 alternating pTSSs this region was defined as 25 bp upstream of the most upstream pTSS and 75 bp
726 downstream of the most downstream pTSS. HTSeq-count (101) was used to count reads mapping to

727 genomic regions described above for both the RNA- and CAGE-seq sample datasets. The raw read
728 counts were then used to analyse differential expression across these regions between the time-
729 points using DESeq2 (default normalisation described by Love et al. (47)) and those regions showing
730 changes with an adjusted p-value (padj) of <0.05 were considered significant. A caveat of this 'early'
731 or 'late' definition is that it is a binary definition of whether a gene is up- or downregulated between
732 conditions (time-points), relative to the background read depth of reads, which map to the genome
733 in question. Further analysis of ASFV genes used their characterised or predicted functions, from the
734 VOCS tool database (https://4virology.net/) (102,103) entries for the GRG genome.

735 Quantification of viral genome copies at different time points of infection

736 Porcine lung macrophages were seeded and infected as described above. *Vero* cells were similarly
737 cultured in 6-well plates in DMEM medium supplemented with 10% Fetal calf serum, 100 IU/ml
738 penicillin and 100 µg/ml streptomycin, when semi-confluent they were infected with MOI 5 of
739 Ba71V. Immediately after infection (after 1h adsorption period, considered '0 hpi), or at 5 hpi, and
740 16 hpi, the supernatant was removed and nucleic acids were extracted using the Qiamp viral RNA kit
741 (Qiagen) and quantified using a NanoDrop spectrophotometer (ThermoFisher Scientific). For
742 quantification of viral genome copy equivalents, 50 ng of each nucleic acid sample was used in qPCR
743 with primers and probe targeting the viral capsid gene B646L. As previously described (104),
744 standard curve quantification qPCR was carried out on a Mx3005P system (Agilent Technologies)
745 using the primers CTGCTCATGGTATCAATCTTATCGA and GATACCACAAGATC(AG)GCCGT and probe 5'-
746 (6-carboxyfluorescein [FAM])-CCACGGGAGGAATACCAACCCAGTG-3'-(6-
747 carboxytetramethylrhodamine [TAMRA]).

748 Analysis of mRNA levels by RT-PCR and quantitative real time PCR (qPCR)

749 RNA from GRG or Ba71V infected macrophages, or *Vero* cells respectively, or from uninfected cell
750 controls, was collected at the different time points post-infection with Trizol, as described above.
751 RNA was reverse transcribed (800 ng RNA per sample) using SuperScript III First-Strand Synthesis
752 System for RT-PCR and random hexamers (Invitrogen). For PCR, cDNAs were diluted 1:20 with
753 nuclease free water and 1 µl each sample was amplified in a total volume of 20 µl using Platinum™
754 Green Hot Start PCR Master Mix (Invitrogen) and 200 nM of each primer. Annealing temperatures
755 were tested for each primer pair in gradient PCR to determine the one optimal for amplification.

756 Supplementary Table 7a shows the primers used for each gene target, the amplicon size, PCR
757 reaction conditions, and NCBI accession numbers for sequences used primer design. PCRs were then
758 performed with limited cycles of amplification to have a semi-quantitative comparison of transcript

759 abundance between infection timepoints (by not reaching the maximum product amplification
760 plateau). Amplification products were viewed using 1.5% agarose gel electrophoresis.

761 C315R transcript levels were assessed by qPCR, using housekeeping gene glyceraldehyde-3-
762 phosphate dehydrogenase (GAPDH) expression was used for normalisation. Primer details and the
763 qPCR amplification program are shown in

764 Supplementary Table 7b (GAPDH primers used for *Vero* cells were previously published by
765 Melchjorsen et al., 2009 (105)). Primers were used at 250 nM concentration with Brilliant III Ultra-
766 Fast SYBR® Green QPCR Master Mix (Agilent 600882), 1 µl cDNA in 20 µl (1:20) total reaction
767 volumes, and qPCRs carried out in Mx3005P system (Agilent Technologies). Similar amplification
768 efficiencies (97-102%) for all primers had been observed upon amplification of serially diluted cDNA
769 samples, and the relative expression at each timepoint of infection was calculated using the formula
770 $2^{\Delta Ct}$ ($2^{Ct_GAPDH-Ct_C315R}$).

771 Preparation of supernatant and cell lysis extracts for ELISA and Western blot detection
772 of host proteins

773 Lung macrophage cultures from two donor outbred pigs (same cells used for CAGEseq) were
774 prepared in 6-well plates. Approximately 1.5x 10^6 cells were seeded per well with 3 ml medium
775 (RPMI with penicillin/streptomycin and 10% pig serum) and incubated at 37 degrees 5% CO2
776 overnight. Cultures were washed once with culture medium to remove non-adherent cells and
777 inoculated with MOI 5 of ASFV-Georgia 2007/1 (or left uninfected as control) and centrifuged 1h at
778 600xg 26 degrees (adsorption period). Supernatants from cell cultures were collected immediately
779 after adsorption for obtaining the 0 hpi timepoint and stored at -70 degrees until analysis. Adherent
780 cells were washed twice with cold DPBS (Sigma) and then lysed with 0.12 ml/well cold RIPA buffer
781 (Thermo Scientific) supplemented with protease inhibitors (Halt Protease Inhibitor Cocktail, Thermo
782 Scientific). For 5h and 16h timepoints, the inoculum was removed after adsorption, cells were
783 washed twice in culture medium and returned to the incubator with fresh 3 ml medium per well for
784 the specified times of infection. Supernatants and lysis volumes were collected similarly to the
785 control. Supernatants were analysed for the presence of CCL2 (Porcine CCL2/MCP-1 ELISA Kit, ES2RB
786 Invitrogen), CXCL8 (Quantikine® ELISA, Porcine IL-8/CXCL8 Immunoassay, P8000 R&D) and TNF-α
787 (Quantikine® ELISA, Porcine TNF-α Immunoassay, PTA00 R&D) as recommended by the
788 manufacturers. A volume of 25 µl each lysate was analysed in Western Blot for expression of ISG15
789 (anti-ISG15 antibody ab233071, Abcam; used at 1:1000 dilution), γ-Tubulin (anti-gamma Tubulin
790 antibody ab11321, Abcam; used at 1:1000 dilution); and viral ASFV protein P30 (in-house mouse

791 monoclonal antibody used at 1:500 dilution). Secondary antibodies used were Goat Anti-Rabbit IgG
792 H&L (HRP) (ab205718, Abcam) and Goat Anti-Mouse Immunoglobulins/HRP (P0447, Dako) both at
793 1:2000 dilution. Western blot membranes were revealed using Pierce ECL Western Blotting
794 Substrate (32106, Thermo Scientific). Band densities were quantified using ImageJ (Rasband, W.S.,
795 ImageJ, U. S. National Institutes of Health, Bethesda, Maryland, USA, https://imagej.nih.gov/ij/,
796 1997-2018).

797 ASFV Promoter Motif Analysis

798 DESeq2 results were used to categorise ASFV genes into two simple sub-classes: early; 87 genes
799 downregulated from early to late infection and late; the 78 upregulated from early to late infection.
800 These characterised gene pTSSs were then pooled with the nORF pTSSs, and sequences upstream
801 and downstream of the pTSS were extracted from the GRG genome in FASTA format using BEDtools.
802 Sequences 35 bp upstream of and including the pTSSs were analysed using MEME software
803 (http://meme-suite.org) (106), searching for 5 motifs with a maximum width of 20 nt and 27 nt,
804 respectively (other settings at default). The input for MEME motif searches included sequences
805 upstream of 134 early pTSSs (87 genes and 47 nORFs) for early promoter searching, while 234 late
806 pTSSs (78 genes and 156 nORFs) were used to search for late promoters. For analysis of conserved
807 motifs upstream of the five clusters described in Figure 6a-b, sequences were extracted in the same
808 manner as above, but grouped according to their cluster. MEME motif searches were carried out for
809 sequences in each cluster, searching for 3 motifs, 5-36 bp in length, with zero or one occurrence per
810 sequence ('zoops' mode).

811 Identification of TSSs by rapid amplification of cDNA ends - 5'RACE

812 For 5'RACE of GRG genes DP146L, pNG4 and CP204L we designed the gene specific primers (GSP)
813 shown in

814 Supplementary Table 7c, and used the kit: "5´ RACE System for Rapid Amplification of cDNA Ends"
815 (Invitrogen), according to manufacturer instructions. Briefly, 150 ng RNA from either 5 hpi or 16 hpi
816 macrophages (one of the replicate RNA samples used for CAGE-seq) was used for cDNA synthesis
817 with GSP1 primers, followed by degradation of the mRNA template with RNase Mix, and column
818 purification of the cDNA. A homopolymeric tail was added to the cDNA 3'ends with Terminal
819 deoxynucleotidyl transferase, which allowed PCR amplification with an "Abridged Anchor Primer"
820 (AAP) from the 5'RACE kit and a nested GSP2 primer. A second PCR was performed over an aliquot
821 of the previous, with 5'RACE "Abridged Universal amplification Primer" (AUAP), and an additional
822 nested primer GSP3, except for pNG4 where GSP2 was re-used due to the small predicted size of the

823 amplicon. Platinum™ Green Hot Start PCR Master Mix (Invitrogen) was used for PCR and products
824 were run in 2% agarose gel electrophoresis (see

825 Supplementary Table 7c for expected sizes). Efficient recovery of cDNA from the purification column
826 requires a product of at least 200 bases and therefore, due to the small predicted size of pNG4
827 transcripts its GSP1 primer was extended at the 5' end with an irrelevant non-annealing sequence of
828 extra 50 nt in order to create a longer recoverable product.

829 CAGE-seq Analysis for the *Sus scrofa* Genome

830 Analyses of TSS-mapping, gene expression and motif searching with CAGE-seq reads mapped to the
831 *Sus scrofa* 11.1 genome were carried out by DNAFORM (Yokohama, Kanagawa, Japan). The 5' ends
832 of CAGE-seq reads were utilised as input for the Reclu pipeline (107) with a cutoff of 0.1 RPM, and
833 irreproducible discovery rate of 0.1. 37,159 total CAGE-seq peaks could be identified, of which
834 around half (16,720) match unique CAGE peaks previously identified by Roberts et al. (64) (i.e. within
835 100 nt of any of them). TSSs for 9,384 protein-coding genes (out of 21,288) were annotated de novo
836 from the CAGE-defined TSSs (Supplementary Table 4).

837 Protein-coding genes with annotated TSSs (9,384 out of 21,288) were then subjected to differential
838 expression analysis. CAGE-seq reads were summed up over all TSSs assigned to a gene and
839 compared between two time points using edgeR (108) at maximum false discovery rate of 0.05. The
840 full list of host genes with annotated promoters together with their estimated expression levels is
841 provided in Supplementary Table 5. Gene set enrichment analysis was performed with the DAVID 6.8
842 Bioinformatics Resources (109), using best BLASTP (110) human hits (from the UniProt (111)
843 reference human proteome). The 9,331 genes with human homologs were used as a background,
844 and functional annotations of the four major expression response groups (late/early up-/down-
845 regulated genes) were clustered in DAVID 6.8 using medium classification stringency. MEME motif
846 searches were conducted for promoters of four differentially regulated subsets of host genes, as
847 defined in Figure 11a. Promoters sequences were extended 1000 bp upstream and 200 bp
848 downstream of TSSs, searched with MEME (max. 10 motifs, max. 100 bp long, on a given strand only,
849 zero or one site per sequence, E < 0.01), and then compared against known vertebrate DNA motifs
850 with Tomtom (p-value < 0.01).

851 Data Availability

852 Raw sequencing data are available on the Sequence Read Archive (SRA) database under BioProject:
853 PRJNA739166. This also includes CAGE-seq data aligned to the ASFV-GRG (FR682468.1 *Sus scrofa*

854 (GCF_000003025.6) genomes (see methods above) in BAM format. Available for review via the link
855 below:

856 https://dataview.ncbi.nlm.nih.gov/object/PRJNA739166?reviewer=390lg85cohvh81llto5gr1d22n

857 Acknowledgements

858 Research in the RNAP laboratory at UCL is funded by a Wellcome Investigator Award in Science
859 'Mechanisms and Regulation of RNAP transcription' to FW (WT 207446/Z/17/Z). GC is funded by the
860 Wellcome Trust ISMB 4-year PhD programme 'Macromolecular machines: interdisciplinary training
861 grounds for structural, computational and chemical biology' (WT 108877/B/15/Z). Research in the
862 ASFV group at The Pirbright Institute is funded by the Biotechnology and Biological Sciences
863 Research Council (BBS/E/I/0007030 and BBS/E/I/0007031). The authors are grateful to all members
864 of the RNAP lab and Tine Arnvig for critical reading of the manuscript.

865

866 References

867 1. Gogin A, Gerasimov V, Malogolovkin A, Kolbasov D. African swine fever in the North Caucasus
868 region and the Russian Federation in years 2007-2012. Virus Res. 2013 Apr 1;173(1):198–203.

869 2. Zhou X, Li N, Luo Y, Liu Y, Miao F, Chen T, et al. Emergence of African Swine Fever in China,
870 2018. Transbound Emerg Dis. 2018 Dec 1;65(6):1482–4.

871 3. Alonso C, Borca M, Dixon L, Revilla Y, Rodriguez F, Escribano JM, et al. ICTV Virus Taxonomy
872 Profile: Asfarviridae. J Gen Virol. 2018 May 1;99(5):613–4.

873 4. Koonin E V., Yutin N. Origin and evolution of eukaryotic large nucleo-cytoplasmic DNA viruses.
874 Intervirology. 2010;53(5):284–92.

875 5. Yutin N, Koonin E V. Hidden evolutionary complexity of Nucleo-Cytoplasmic Large DNA
876 viruses of eukaryotes. Virol J. 2012 Aug 14;9(1):161.

877 6. Broyles SS. Vaccinia virus transcription. J Gen Virol. 2003 Sep 1;84(9):2293–303.

878 7. Alejo A, Matamoros T, Guerra M, Andrés G. A proteomic atlas of the African swine fever virus
879 particle. J Virol. 2018 Sep 5;JVI.01293-18.

880 8. Salas ML, Kuznar J, Viñuela E. Polyadenylation, methylation, and capping of the RNA
881 synthesized in vitro by African swine fever virus. Virology. 1981 Sep 1;113(2):484–91.

882 9. Rodríguez JM, Salas ML. African swine fever virus transcription. Vol. 173, Virus Research.

883 Elsevier B.V.; 2013. p. 15–28.

884 10. Cackett G, Matelska D, Sýkora M, Portugal R, Malecki M, Bähler J, et al. The African Swine
885 Fever Virus Transcriptome. J Virol. 2020 Feb 19;94(9).

886 11. Iyer LM, Balaji S, Koonin E V., Aravind L. Evolutionary genomics of nucleo-cytoplasmic large
887 DNA viruses. Virus Res. 2006 Apr;117(1):156–84.

888 12. Yutin N, Wolf YI, Raoult D, Koonin E V. Eukaryotic large nucleo-cytoplasmic DNA viruses:
889 clusters of orthologous genes and reconstruction of viral genome evolution. Virol J. 2009 Dec
890 17;6(3):223.

891 13. Fischer U, Grimm C, Bartuli J, Böttcher B, Szalay A. Structural basis of the complete poxvirus
892 transcription initiation process. 2021 Apr 28;

893 14. Rodríguez JM, Moreno LT, Alejo A, Lacasta A, Rodríguez F, Salas ML. Genome Sequence of
894 African Swine Fever Virus BA71, the Virulent Parental Strain of the Nonpathogenic and
895 Tissue-Culture Adapted BA71V. Munderloh UG, editor. PLoS One. 2015 Nov
896 30;10(11):e0142889.

897 15. Yáñez RJ, Rodríguez JM, Nogal ML, Yuste L, Enríquez C, Rodriguez JF, et al. Analysis of the
898 complete nucleotide sequence of African swine fever virus. Virology. 1995 Apr 1;208(1):249–
899 78.

900 16. Dixon LK, Chapman DAG, Netherton CL, Upton C. African swine fever virus replication and
901 genomics. Virus Res. 2013;173(1):3–14.

902 17. Chapman DAG, Tcherepanov V, Upton C, Dixon LK. Comparison of the genome sequences of
903 non-pathogenic and pathogenic African swine fever virus isolates. J Gen Virol. 2008 Feb
904 1;89(2):397–408.

905 18. Forth JH, Forth LF, King J, Groza O, Hübner A, Olesen AS, et al. A deep-sequencing workflow
906 for the fast and efficient generation of high-quality African swine fever virus whole-genome
907 sequences. Viruses. 2019;11(9).

908 19. Chapman DAG, Darby AC, da Silva M, Upton C, Radford AD, Dixon LK. Genomic analysis of
909 highly virulent Georgia 2007/1 isolate of African swine fever virus. Emerg Infect Dis. 2011
910 Apr;17(4):599–605.

911 20. Farlow J, Donduashvili M, Kokhreidze M, Kotorashvili A, Vepkhvadze NG, Kotaria N, et al.

912 Intra-epidemic genome variation in highly pathogenic African swine fever virus (ASFV) from
913 the country of Georgia. Virol J. 2018 Dec 14;15(1):190.

914 21. Mazur-Panasiuk N, Woźniakowski G, Niemczuk K. The first complete genomic sequences of
915 African swine fever virus isolated in Poland. Sci Rep. 2019 Dec 1;9(1):3–5.

916 22. Granberg F, Torresi C, Oggiano A, Malmberg M, Iscaro C, De Mia GM, et al. Complete genome
917 sequence of an African swine fever virus isolate from Sardinia, Italy. Genome Announc.
918 2016;4(6):1220–36.

919 23. Wang Z, Jia L, Li J, Liu H, Liu D. Pan-Genomic Analysis of African Swine Fever Virus. Virologica
920 Sinica. Science Press; 2019. p. 1–4.

921 24. Rowlands RJ, Michaud V, Heath L, Hutchings G, Oura C, Vosloo W, et al. African swine fever
922 virus isolate, Georgia, 2007. Emerg Infect Dis. 2008 Dec;14(12):1870–4.

923 25. Zhao D, Liu R, Zhang X, Li F, Wang J, Zhang J, et al. Replication and virulence in pigs of the first
924 African swine fever virus isolated in China. Emerg Microbes Infect. 2019 Jan 1;8(1):438–47.

925 26. Zani L, Forth JH, Forth L, Nurmoja I, Leidenberger S, Henke J, et al. Deletion at the 5'-end of
926 Estonian ASFV strains associated with an attenuated phenotype. Sci Reports 2018 81. 2018
927 Apr 25;8(1):1–11.

928 27. Gallardo C, Nurmoja I, Soler A, Delicado V, Simón A, Martin E, et al. Evolution in Europe of
929 African swine fever genotype II viruses from highly to moderately virulent. Vet Microbiol.
930 2018 Jun 1;219:70–9.

931 28. Pershin A, Shevchenko I, Igolkin A, Zhukov I, Mazloum A, Aronova E, et al. A Long-Term Study
932 of the Biological Properties of ASF Virus Isolates Originating from Various Regions of the
933 Russian Federation in 2013–2018. Vet Sci 2019, Vol 6, Page 99. 2019 Dec 6;6(4):99.

934 29. Sun E, Zhang Z, Wang Z, He X, Zhang X, Wang L, et al. Emergence and prevalence of naturally
935 occurring lower virulent African swine fever viruses in domestic pigs in China in 2020. Sci
936 China Life Sci. 2021 May 1;64(5):752–65.

937 30. Imbery J, Upton C. Organization of the multigene families of African Swine Fever Virus. Fine
938 Focus. 2017;3(2):155–70.

939 31. Netherton CL, Connell S, Benfield CTO, Dixon LK. The Genetics of Life and Death: Virus-Host
940 Interactions Underpinning Resistance to African Swine Fever, a Viral Hemorrhagic Disease.

941 Front Genet. 2019 May 3;10(MAY):402.

942 32. Reis AL, Abrams CC, Goatley LC, Netherton C, Chapman DG, Sanchez-Cordon P, et al. Deletion
943 of African swine fever virus interferon inhibitors from the genome of a virulent isolate
944 reduces virulence in domestic pigs and induces a protective response. Vaccine. 2016 Sep
945 7;34(39):4698–705.

946 33. O'Donnell V, Risatti GR, Holinka LG, Krug PW, Carlson J, Velazquez-Salinas L, et al.
947 Simultaneous Deletion of the 9GL and UK Genes from the African Swine Fever Virus Georgia
948 2007 Isolate Offers Increased Safety and Protection against Homologous Challenge. J Virol.
949 2017 Jan;91(1).

950 34. Li D, Zhang J, Yang W, Li P, Ru Y, Kang W, et al. African swine fever virus protein MGF-505-7R
951 promotes virulence and pathogenesis by inhibiting JAK1- and JAK2-mediated signaling. J Biol
952 Chem. 2021 Nov;297(5):101190.

953 35. Li D, Liu YY, Qi X, Wen Y, Li P, Ma Z, et al. African Swine Fever Virus MGF-110-9L-deficient
954 Mutant Has Attenuated Virulence in Pigs. Virol Sin. 2021 Apr 1;36(2):187–95.

955 36. Keßler C, Forth JH, Keil GM, Mettenleiter TC, Blome S, Karger A. The intracellular proteome of
956 African swine fever virus. Sci Rep. 2018 Oct 2;8(1):14714.

957 37. Randall RE, Goodbourn S. Interferons and viruses: An interplay between induction, signalling,
958 antiviral responses and virus countermeasures. Vol. 89, Journal of General Virology.
959 Microbiology Society; 2008. p. 1–47.

960 38. Afonso RCL, Piccone ME, Zaffuto KM, Neilan J, Kutish GF, Lu Z, et al. African swine fever virus
961 multigene family 360 and 530 genes affect host interferon response. J Virol. 2004;78:1858–
962 64.

963 39. Neilan JG, Zsak L, Lu Z, Kutish GF, Afonso CL, Rock DL. Novel Swine Virulence Determinant in
964 the Left Variable Region of the African Swine Fever Virus Genome. J Virol. 2002 Apr
965 1;76(7):3095–104.

966 40. Golding JP, Goatley L, Goodbourn S, Dixon LK, Taylor G, Netherton CL. Sensitivity of African
967 swine fever virus to type I interferon is linked to genes within multigene families 360 and 505.
968 Virology. 2016 Jun 1;493:154–61.

969 41. Mosser DM, Edwards JP. Exploring the full spectrum of macrophage activation. Vol. 8, Nature
970 Reviews Immunology. NIH Public Access; 2008. p. 958–69.

971 42. Zhu JJ, Ramanathan P, Bishop EA, O'Donnell V, Gladue DP, Borca M V. Mechanisms of African
972 swine fever virus pathogenesis and immune evasion inferred from gene expression changes
973 in infected swine macrophages. PLoS One. 2019;14(11).

974 43. Jaing C, Rowland RRR, Allen JE, Certoma A, Thissen JB, Bingham J, et al. Gene expression
975 analysis of whole blood RNA from pigs infected with low and high pathogenic African swine
976 fever viruses. Sci Rep. 2017 Dec 31;7(1):10115.

977 44. Fan W, Cao Y, Jiao P, Yu P, Zhang H, Chen T, et al. Synergistic effect of the responses of
978 different tissues against African swine fever virus. Transbound Emerg Dis. 2021;

979 45. Ju X, Li F, Li J, Wu C, Xiang G, Zhao X, et al. Genome-wide transcriptomic analysis of highly
980 virulent African swine fever virus infection reveals complex and unique virus host interaction.
981 Vet Microbiol. 2021 Oct 1;261:109211.

982 46. Yang B, Shen C, Zhang D, Zhang T, Shi X, Yang J, et al. Mechanism of interaction between virus
983 and host is inferred from the changes of gene expression in macrophages infected with
984 African swine fever virus CN/GS/2018 strain. Virol J. 2021 Dec 1;18(1).

985 47. Love MI, Huber W, Anders S. Moderated estimation of fold change and dispersion for RNA-
986 seq data with DESeq2. Genome Biol. 2014 Dec 5;15(12):550.

987 48. Hammond JM, Kerr SM, Smith GL, Dixon LK. An African swine fever virus gene with homology
988 to DNA ligases. Nucleic Acids Res. 1992 Jun 11;20(11):2667–71.

989 49. Reis AL, Goatley LC, Jabbar T, Sanchez-Cordon PJ, Netherton CL, Chapman DAG, et al.
990 Deletion of the African Swine Fever Virus Gene DP148R Does Not Reduce Virus Replication in
991 Culture but Reduces Virus Virulence in Pigs and Induces High Levels of Protection against
992 Challenge. J Virol. 2017 Dec 15;91(24).

993 50. Yang Z, Martens CA, Bruno DP, Porcella SF, Moss B. Pervasive initiation and 3'-end formation
994 of poxvirus postreplicative RNAs. J Biol Chem. 2012 Sep 7;287(37):31050–60.

995 51. Frouco G, Freitas FB, Coelho J, Leitão A, Martins C, Ferreira F. DNA-Binding Properties of
996 African Swine Fever Virus pA104R, a Histone-Like Protein Involved in Viral Replication and
997 Transcription. J Virol. 2017;91(12).

998 52. Conesa A, Madrigal P, Tarazona S, Gomez-Cabrero D, Cervera A, McPherson A, et al. A survey
999 of best practices for RNA-seq data analysis. Genome Biol. 2016 Jan 26;17:13.

1000 53. García-Escudero R, Viñuela E. Structure of African Swine Fever Virus Late Promoters:
1001 Requirement of a TATA Sequence at the Initiation Region. J Virol. 2000 Sep 1;74(17):8176–82.

1002 54. Bailey TL, Boden M, Buske FA, Frith M, Grant CE, Clementi L, et al. MEME SUITE: tools for
1003 motif discovery and searching. Nucleic Acids Res. 2009 Jul 1;37(Web Server):W202–8.

1004 55. Gupta S, Stamatoyannopoulos JA, Bailey TL, Noble W. Quantifying similarity between motifs.
1005 Genome Biol. 2007 Feb 26;8(2):R24.

1006 56. Rodríguez JM, Salas ML, Viñuela E. Intermediate class of mRNAs in African swine fever virus. J
1007 Virol. 1996 Dec;70(12):8584–9.

1008 57. Kim DE, Chivian D, Baker D. Protein structure prediction and analysis using the Robetta
1009 server. Nucleic Acids Res. 2004;32(WEB SERVER ISS.):W526–31.

1010 58. Vydelingum S, Baylis SA, Bristow C, Smith GL, Dixon LK. Duplicated genes within the variable
1011 right end of the genome of a pathogenic isolate of African swine fever virus. J Gen Virol. 1993
1012 Oct 1;74(10):2125–30.

1013 59. Zhang J, Zhang Y, Chen T, Yang JJ, Yue H, Wang L, et al. Deletion of the L7L-L11L Genes
1014 Attenuates ASFV and Induces Protection against Homologous Challenge. Viruses. 2021 Feb
1015 1;13(2).

1016 60. Krug PW, Holinka LG, O'Donnell V, Reese B, Sanford B, Fernandez-Sainz I, et al. The
1017 Progressive Adaptation of a Georgian Isolate of African Swine Fever Virus to Vero Cells Leads
1018 to a Gradual Attenuation of Virulence in Swine Corresponding to Major Modifications of the
1019 Viral Genome. J Virol. 2015 Feb 15;89(4):2324–32.

1020 61. Kelley LA, Mezulis S, Yates CM, Wass MN, Sternberg MJE. The Phyre2 web portal for protein
1021 modeling, prediction and analysis. Nat Protoc. 2015 May 7;10(6):845–58.

1022 62. Liu H, Li L, Voss C, Wang F, Liu J, Li SSC. A Comprehensive Immunoreceptor Phosphotyrosine-
1023 based Signaling Network Revealed by Reciprocal Protein–Peptide Array Screening. Mol Cell
1024 Proteomics. 2015 Jul 1;14(7):1846–58.

1025 63. Gabler F, Nam SZ, Till S, Mirdita M, Steinegger M, Söding J, et al. Protein Sequence Analysis
1026 Using the MPI Bioinformatics Toolkit. Curr Protoc Bioinforma. 2020 Dec 1;72(1).

1027 64. Robert C, Kapetanovic R, Beraldi D, Watson M, Archibald AL, Hume DA. Identification and
1028 annotation of conserved promoters and macrophage-expressed genes in the pig genome.

1029 BMC Genomics. 2015 Nov 18;16(1).

1030 65. Ganchi PA, Sun SC, Greene WC, Ballard DW. A novel NF-kappa B complex containing p65
1031 homodimers: implications for transcriptional control at the level of subunit dimerization. Mol
1032 Cell Biol. 1993 Dec;13(12):7826–35.

1033 66. Dixon LK, Abrams CC, Bowick G, Goatley LC, Kay-Jackson PC, Chapman D, et al. African swine
1034 fever virus proteins involved in evading host defence systems. In: Veterinary Immunology and
1035 Immunopathology. 2004. p. 117–34.

1036 67. Powell PP, Dixon LK, Parkhouse RM. An IkappaB homolog encoded by African swine fever
1037 virus provides a novel mechanism for downregulation of proinflammatory cytokine responses
1038 in host macrophages. J Virol. 1996;70(12):8527–33.

1039 68. Granja AG, Sánchez EG, Sabina P, Fresno M, Revilla Y. African swine fever virus blocks the
1040 host cell antiviral inflammatory response through a direct inhibition of PKC-theta-mediated
1041 p300 transactivation. J Virol. 2009 Jan 15;83(2):969–80.

1042 69. Nogal ML, González de Buitrago G, Rodríguez C, Cubelos B, Carrascosa AL, Salas ML, et al.
1043 African swine fever virus IAP homologue inhibits caspase activation and promotes cell
1044 survival in mammalian cells. J Virol. 2001 Mar 15;75(6):2535–43.

1045 70. Takeya T, Hanafusa H. DNA sequence of the viral and cellular src gene of chickens. II.
1046 Comparison of the src genes of two strains of avian sarcoma virus and of the cellular
1047 homolog. J Virol. 1982;44(1):12–8.

1048 71. Kaneko T, Stogios PJ, Ruan X, Voss C, Evdokimova E, Skarina T, et al. Identification and
1049 characterization of a large family of superbinding bacterial SH2 domains. Nat Commun. 2018
1050 Dec 1;9(1).

1051 72. Liu Y, Li Y, Xie Z, Ao Q, Di D, Yu W, et al. Development and in vivo evaluation of MGF100-1R
1052 deletion mutant in an African swine fever virus Chinese strain. Vet Microbiol. 2021 Oct 1;261.

1053 73. Vuono E, Ramirez-Medina E, Pruitt S, Rai A, Silva E, Espinoza N, et al. Evaluation in swine of a
1054 recombinant georgia 2010 african swine fever virus lacking the i8l gene. Viruses. 2021 Jan
1055 1;13(1).

1056 74. Camacho A, ViÑuela E. Protein p22 of African swine fever virus: An early structural protein
1057 that is incorporated into the membrane of infected cells. Virology. 1991 Mar 1;181(1):251–7.

1058 75. Netherton C, Rouiller I, Wileman T. The subcellular distribution of multigene family 110
1059 proteins of African swine fever virus is determined by differences in C-terminal KDEL
1060 endoplasmic reticulum retention motifs. J Virol. 2004 Apr 1;78(7):3710–21.

1061 76. Ramirez-Medina E, Vuono E, Pruitt S, Rai A, Silva E, Espinoza N, et al. Development and In
1062 Vivo Evaluation of a MGF110-1L Deletion Mutant in African Swine Fever Strain Georgia.
1063 Viruses. 2021 Feb 1;13(2).

1064 77. Cackett G, Sýkora M, Werner F. Transcriptome view of a killer: African swine fever virus. Vol.
1065 48, Biochemical Society Transactions. Portland Press Ltd; 2020. p. 1569–81.

1066 78. Quintas A, Pérez-Núñez D, Sánchez EG, Nogal ML, Hentze MW, Castelló A, et al.
1067 Characterization of the African Swine Fever Virus Decapping Enzyme during Infection. Jung
1068 JU, editor. J Virol. 2017 Dec 15;91(24):e00990-17.

1069 79. Kunsch C, Ruben SM, Rosen CA. Selection of optimal kappa B/Rel DNA-binding motifs:
1070 interaction of both subunits of NF-kappa B with DNA is required for transcriptional activation.
1071 Mol Cell Biol. 1992 Oct;12(10):4412–21.

1072 80. Gómez del Moral M, Ortuño E, Fernández-Zapatero P, Alonso F, Alonso C, Ezquerra A, et al.
1073 African Swine Fever Virus Infection Induces Tumor Necrosis Factor Alpha Production:
1074 Implications in Pathogenesis. J Virol. 1999 Mar 1;73(3):2173–80.

1075 81. Roy S, Schmeier S, Arner E, Alam T, Parihar SP, Ozturk M, et al. Redefining the transcriptional
1076 regulatory dynamics of classically and alternatively activated macrophages by deepCAGE
1077 transcriptomics. Nucleic Acids Res. 2015;43(14):6969–82.

1078 82. Castelló A, Quintas A, Sánchez EG, Sabina P, Nogal M, Carrasco L, et al. Regulation of host
1079 translational machinery by African swine fever virus. PLoS Pathog. 2009 Aug;5(8):e1000562.

1080 83. Sánchez EG, Quintas A, Nogal M, Castelló A, Revilla Y. African swine fever virus controls the
1081 host transcription and cellular machinery of protein synthesis. Virus Res. 2013 Apr
1082 1;173(1):58–75.

1083 84. Barrado-Gil L, Del Puerto A, Muñoz-Moreno R, Galindo I, Cuesta-Geijo MA, Urquiza J, et al.
1084 African Swine Fever Virus Ubiquitin-Conjugating Enzyme Interacts With Host Translation
1085 Machinery to Regulate the Host Protein Synthesis. Front Microbiol. 2020 Dec 15;11.

1086 85. Gschwandtner M, Derler R, Midwood KS. More Than Just Attractive: How CCL2 Influences
1087 Myeloid Cell Behavior Beyond Chemotaxis. Front Immunol. 2019 Dec 13;0:2759.

1088 86. Xia C, Braunstein Z, Toomey AC, Zhong J, Rao X. S100 proteins as an important regulator of
1089 macrophage inflammation. Vol. 8, Frontiers in Immunology. Frontiers Media S.A.; 2018.

1090 87. Yang Z, Bruno DP, Martens CA, Porcella SF, Moss B. Simultaneous high-resolution analysis of
1091 vaccinia virus and host cell transcriptomes by deep RNA sequencing. Proc Natl Acad Sci U S A.
1092 2010 Jun 22;107(25):11513–8.

1093 88. Olasz F, Tombácz D, Torma G, Csabai Z, Moldován N, Dörmő Á, et al. Short and Long-Read
1094 Sequencing Survey of the Dynamic Transcriptomes of African Swine Fever Virus and the Host
1095 Cells. Front Genet. 2020 Jul 28;11:2020.02.27.967695.

1096 89. Torma G, Tombácz D, Csabai Z, Moldován N, Mészáros I, Zádori Z, et al. Combined short and
1097 long-read sequencing reveals a complex transcriptomic architecture of African swine fever
1098 virus. Viruses. 2021 Apr 1;13(4).

1099 90. Yang Z, Bruno DP, Martens CA, Porcella SF, Moss B. Genome-Wide Analysis of the 5' and 3'
1100 Ends of Vaccinia Virus Early mRNAs Delineates Regulatory Sequences of Annotated and
1101 Anomalous Transcripts. J Virol. 2011 Jun;85(12):5897–909.

1102 91. Gershon PD, Moss B. Early transcription factor subunits are encoded by vaccinia virus late
1103 genes. Proc Natl Acad Sci U S A. 1990 Jun 1;87(11):4401–5.

1104 92. Li J, Broyles SS. Recruitment of vaccinia virus RNA polymerase to an early gene promoter by
1105 the viral early transcription factor. J Biol Chem. 1993;268(4):2773–80.

1106 93. Patikoglou GA, Kim JL, Sun L, Yang SH, Kodadek T, Burley SK. TATA element recognition by the
1107 TATA box-binding protein has been conserved throughout evolution. Genes Dev. 1999 Dec
1108 15;13(24):3217–30.

1109 94. Andrews S. FastQC A Quality Control tool for High Throughput Sequence Data. Babraham,
1110 England: Babraham Bioinformatics;

1111 95. Langmead B, Salzberg SL. Fast gapped-read alignment with Bowtie 2. Nat Methods. 2012 Apr
1112 4;9(4):357–9.

1113 96. Kim D, Langmead B, Salzberg SL. HISAT: a fast spliced aligner with low memory requirements.
1114 Nat Methods. 2015 Apr 9;12(4):357–60.

1115 97. Quinlan AR, Hall IM. BEDTools: a flexible suite of utilities for comparing genomic features.
1116 Bioinformatics. 2010 Mar 15;26(6):841–2.

1117 98. RStudio Team. RStudio: Integrated Development for R. Boston, MA: RStudioe, Inc; 2016.

1118 99. Huber W, Carey VJ, Gentleman R, Anders S, Carlson M, Carvalho BS, et al. Orchestrating high-
1119 throughput genomic analysis with Bioconductor. Nat Methods. 2015 Feb 1;12(2):115–21.

1120 100. Thodberg M, Thieffry A, Vitting-Seerup K, Andersson R, Sandelin A. CAGEfightR: Analysis of 5'-
1121 end data using R/Bioconductor. BMC Bioinformatics. 2019 Oct 4;20(1):487.

1122 101. Anders S, Pyl PT, Huber W. HTSeq--a Python framework to work with high-throughput
1123 sequencing data. Bioinformatics. 2015 Jan 15;31(2):166–9.

1124 102. Upton C, Slack S, Hunter AL, Ehlers A, Roper RL, Rock DL. Poxvirus orthologous clusters:
1125 toward defining the minimum essential poxvirus genome. J Virol. 2003 Jul 1;77(13):7590–600.

1126 103. Tu SL, Upton C. Bioinformatics for Analysis of Poxvirus Genomes. In: Methods in Molecular
1127 Biology. Humana Press Inc.; 2019. p. 29–62.

1128 104. DP K, SM R, GH H, SS G, PJ W, LK D, et al. Development of a TaqMan PCR assay with internal
1129 amplification control for the detection of African swine fever virus. J Virol Methods. 2003
1130 Jan;107(1):53–61.

1131 105. Melchjorsen J, Kristiansen H, Christiansen R, Rintahaka J, Matikainen S, Paludan SR, et al.
1132 Differential regulation of the OASL and OAS1 genes in response to viral infections. J Interf
1133 Cytokine Res. 2009 Apr 1;29(4):199–207.

1134 106. Bailey TL, Elkan C. Fitting a mixture model by expectation maximization to discover motifs in
1135 biopolymers. Proceedings Int Conf Intell Syst Mol Biol. 1994;2:28–36.

1136 107. Ohmiya H, Vitezic M, Frith MC, Itoh M, Carninci P, Forrest ARR, et al. RECLU: A pipeline to
1137 discover reproducible transcriptional start sites and their alternative regulation using capped
1138 analysis of gene expression (CAGE). BMC Genomics. 2014 Apr 25;15(1):269.

1139 108. Robinson MD, McCarthy DJ, Smyth GK. edgeR: A Bioconductor package for differential
1140 expression analysis of digital gene expression data. Bioinformatics. 2009 Nov 11;26(1):139–
1141 40.

1142 109. Huang DW, Sherman BT, Lempicki RA. Systematic and integrative analysis of large gene lists
1143 using DAVID bioinformatics resources. Nat Protoc. 2009;4(1):44–57.

1144 110. Altschul SF, Gish W, Miller W, Myers EW, Lipman DJ. Basic local alignment search tool. J Mol
1145 Biol. 1990 Oct 5;215(3):403–10.

1146 111. Bateman A. UniProt: A worldwide hub of protein knowledge. Nucleic Acids Res. 2019 Jan
1147 8;47(D1):D506–15.

1148 112. Ramírez F, Dündar F, Diehl S, Grüning BA, Manke T. deepTools: a flexible platform for
1149 exploring deep-sequencing data. Nucleic Acids Res. 2014 Jul;42(Web Server issue):W187-91.

1150 113. Crooks GE, Hon G, Chandonia JM, Brenner SE. WebLogo: A sequence logo generator. Genome
1151 Res. 2004 May 12;14(6):1188–90.

1152 114. Grant CE, Bailey TL, Noble WS. FIMO: scanning for occurrences of a given motif.
1153 Bioinformatics. 2011 Apr 1;27(7):1017–8.

1154 115. McCarthy DJ, Chen Y, Smyth GK. Differential expression analysis of multifactor RNA-Seq
1155 experiments with respect to biological variation. Nucleic Acids Res. 2012 May 1;40(10):4288–
1156 97.

1157 116. Benjamini Y, Hochberg Y. Controlling the False Discovery Rate: A Practical and Powerful
1158 Approach to Multiple Testing. J R Stat Soc Ser B. 1995 Jan;57(1):289–300.

1159 117. Yates AD, Achuthan P, Akanni W, Allen J, Allen J, Alvarez-Jarreta J, et al. Ensembl 2020.
1160 Nucleic Acids Res. 2020 Jan 1;48(D1):D682–8.

1161 118. Wheeler DL, Church DM, Federhen S, Lash AE, Madden TL, Pontius JU, et al. Database
1162 resources of the National Center for Biotechnology. Nucleic Acids Res. 2003 Jan 1;31(1):28–
1163 33.

1164

1165 Figures

1166

1167 Figure 1. Functional genome annotation of ASFV GRG. (a) Comparison between the genomes of
1168 BA71V and GRG, generated with Circos (http://circos.ca/). Blue lines represent sequence
1169 conservation (Blast E-values per 100 nt). The Inner ring represents genes defined as MGF members
1170 (purple), and all others (grey). The outer ring shows annotated genes which we have defined as early
1171 or late according to downregulation or upregulation between 5 hpi and 16 hpi from DESeq2 analysis.
1172 (b) 189 GRG annotated ORFs are represented as arrows and coloured according to strand. CAGE-seq
1173 peaks across the GRG genome at 5 hpi (c) and 16 hpi (d), normalized coverage reads per million
1174 mapped reads (RPM) of 5' ends of CAGE-seq reads. The coverage was capped at 20000 RPM for
1175 visualisation, though multiple peaks exceeded this. DeepTools (112), was used to convert bam files

1176 to bigwig format and imported into Rstudio for visual representation via packages ggplot, ggbio,
1177 rtracklayer, and gggenes was used to generate the ORF map in (b).

1178

1179 Figure 2. Summary of GRG gene expression (a) Expression profiles for 164 genes for which we
1180 annotated pTSSs from CAGE-seq and which showed significant differential expression. Log2 fold
1181 change and basemean expression values were from DESeq2 analysis of raw counts (see methods).
1182 Genes are coloured according to their log2 fold change in expression as red (positive: upregulated
1183 from 5 hpi to 16 hpi) or blue (negative: downregulated). MGFs are emphasised with a black outline
1184 to highlight their overrepresentation in the group of downregulated genes. (b) Expression profiles
1185 for 41 genes (excluding nORFs) only detected as being expressed in GRG and not BA71V, format as in
1186 (a). (c) Expression (RPM) of 20 highest-expressed genes at 5 hpi, error bars represent standard
1187 deviation between replicates. (d) Expression (RPM) of 20 highest-expressed genes at 16 hpi pi, error
1188 bars are the standard deviation between replicates.

1189

1190 Figure 3. Comparison of gene expression profiles for genes shared between GRG and BA71V. Scatter
1191 plots of mean RPM across replicates for shared genes at 5 hpi (a) and 16 hpi (b), coloured according
1192 to whether genes show significant downregulation (blue), or upregulation (red) according to DESeq2
1193 analysis in GRG. In both (b) and (c) genes with RPM values above 40000 RPM in either strain are
1194 labelled. (c) Comparison of log2 fold change in expression values of genes in GRG and BA71V, in blue
1195 are downregulated (early) genes in both strains, red are upregulated (late) genes in both strains,
1196 while the genes which disagree in their differential expression patterns between strains are in black.
1197 R represents the Pearson Correlation coefficient for each individual plot in (a), (b), and (c). Due to
1198 inconsistencies in their genome annotations, two genes were omitted from the BA71V-GRG
1199 transcriptome comparisons in Figures 2b and 3a-d: EP296R in GRG known as E296R in BA71V, and
1200 C122R (GRG) is the old nomenclature for C105R (BA71V), which are now correctly named in
1201 Supplementary Table 1e and Figure 2a. Both genes showed the same early expression patterns in
1202 BA71V (10) and GRG (Supplementary Table 1e) so would strengthen the patterns observed.

1203

1204 Figure 4. Increase in virus genome copy number mRNA levels during late infection. (a) The 'log2
1205 change' represents log2 of the ratio of CAGE-seq reads (normalised per million mapped reads) at 16
1206 hpi vs. 5 hpi per nucleotide across the genome. Alignment comparisons and calculations were done

1207 with deepTools (112). (b) Replicate means of CAGE-seq reads mapped to either the BA71V (green) or
1208 GRG (purple) genomes throughout infection. (c) Fold change in CAGE-seq reads during infection,
1209 calculated via mean value across 2 replicates, but with the assumption number of reads at 0 hpi is 0,
1210 therefore dividing by values from 5 hpi. (d) Change in genome copies from DNA qPCR of B646L gene,
1211 dividing by value at 0 hpi to represent '1 genome copy per infected cell'. (e) Fold change in genome
1212 copies present at 0 hpi , 5 hpi and 16 hpi from qPCR in (d). (d) calculated as for (c), but with actual
1213 vales for 0 hpi.

1214

1215 Figure 5. RT-PCR results of genes for comparison to CAGE-seq data from (a) MGF 505-7R, (b) NP419L,
1216 (c) D345L, (d) MGF 360-12L, (e) MGF 505-9R, and (f) qRT-PCR results of C315R (ASFV-TFIIB). (NT = no
1217 template control). For each panel at the top is a diagrammatic representation of each gene's TSSs
1218 (bent arrow, including both pTSS and ioTSSs), annotated ORF (red arrow), and arrow pairs in cyan or
1219 yellow represent the primers used for PCR (see methods for primer sequences). Beneath each PCR
1220 results are bar charts representing the CAGE-seq results as either normalised (mean RPM) or raw
1221 (mean read counts) data, error bars show the range of values from each replicate.

1222

1223 Figure 6. Comparison of the raw read counts for genes shared between BA71V and GRG. (a)
1224 clustered heatmap representation of raw counts for genes shared between BA71V and GRG,
1225 generated with pheatmap. (b) broad patterns represented by genes in the 5 clusters indicated in (a).
1226 (c) histogram showing the percentage of the total raw reads per gene which are detected at 16 hpi
1227 vs. 5 hpi post-infection, and comparing the distribution of percentages between GRG and BA71V. (d)
1228 Mean read counts from GRG at 5 hpi vs 16 hpi replicates, showing a significant increase (T-test, p-
1229 value: 0.045) from 5 hpi to 16 hpi.

1230

1231 Figure 7. Promoter motifs and initiators detected in early and late ASFV GRG TSSs including
1232 alternative TSSs and those for nORFs. (a) Consensus of 30 bp upstream and 5 bp downstream of all
1233 134 early TSSs including nORFs, with the conserved EPM (10) and Inr annotated. (b) 30 bp upstream
1234 and 5 bp downstream of all 234 late gene and nORFs TSSs, with the LPM and Inr annotated (c) The
1235 conserved EPM detected via MEME motif search of 35 bp upstream for 133 for 134 early TSSs (E-
1236 value: 3.1e-069). The conserved LPM detected via MEME motif search of 35 bp upstream for 46 for
1237 234 late gene TSSs (E-value: 2.6e-003). The locations of the EPM shown in (b) and LPM shown in (d)

1238 are annotated with brackets in (a) and (b), respectively. Motifs detected via MEME search of 35 bp
1239 upstream of genes in clusters from Figure 6: cluster 1 (7 genes, E-value: 9.1e-012), 2 (15 genes, E-
1240 value: 2.6e-048), 3 (60 genes, E-value: 1.0e-167), 4 (32 genes, E-value: 4.7e-105), 5 (16 genes, E-
1241 value: 5.7e-036), are shown in e-i, respectively. For ease of comparison, (e), (g), (i) and (f), (h) are
1242 aligned at TSS position. All motifs were generated using Weblogo 3 (113). (k) shows the distribution
1243 of MEME motif-end distances, from last nt (in coloured bracket), to their respective downstream
1244 TSSs.

1245

1246 Figure 8. The TSSs of MGF 360-19R. Panels (a) 5 hpi and (b) 16 hpi show CAGE-seq 5' end data from
1247 these time-points, in red are reads from the plus strand and blue from the minus strand, the RPM
1248 scales are on the right. (c) TSSs are annotated with arrows if they can generate a minimum of 5
1249 residue-ORF downstream, and grey bars indicate where they are located on the CAGE-seq coverage
1250 in (a) and (b). ORFs identified downstream of TSSs are shown as red arrows (visualized with R
1251 package gggenes), including three short nORFs out of frame with MGF 360-19R. Also shown are
1252 three in-frame truncation variants, from TSSs detected inside the full-length MGF 360-19R 269-
1253 residue ORF, downstream of its pTSS at 185213. Blue or yellow boxes upstream of TSSs indicate
1254 whether the EPM or LPM (respectively) could be detected within 35 nt upstream of the TSS using
1255 FIMO searching (114).

1256

1257 Figure 9. Summary of intra-ORF TSSs (ioTSSs) and nORFs detected in the GRG genome, further
1258 information in Supplementary Table 2. (a) Summarises the gene types in which ioTSSs were
1259 detected, showing an overrepresentation of MGFs, especially from families 360 and 505,
1260 furthermore, the majority of ioTSSs are detected at 16 hpi. (b) For ioTSSs in-frame with the original,
1261 summarised are the subsequent UTR lengths i.e. distance from TSS to next in frame ATG start codon,
1262 which could generate a truncation variant. (c) Example of a miss-annotation for CP204L, whereby
1263 the pTSS is downstream the predicted start codon. (d) and (e) show the results of 5'RACE for three
1264 genes (DP146L, pNG4, and CP204L, see methods for primers), at 5 hpi and 16 hpi, respectively.
1265 Examples of genome regions around DP146L (f) and pNG4 (g), wherein ioTSSs were detected with
1266 capacity for altering ORF length in subsequent transcripts, and therefore protein output. Primers
1267 used for 5'RACE for DP146L and pNG4 are represented as black arrows in (f) and (g), respectively.

1268

1269 Figure 10. MGF 100 genes likely encode SH2-domain factors. (a) Occurrence of MGF 100 genes in
1270 selected ASFV strains, with genotype and pathogenicity indicated (as yes. Y, or no, N). '1L/2L' refers
1271 to the gene MGF 100-2L (DP141L in BA71V) and MGF 100-1L in the FR682468.1 genome annotation.
1272 (b) The top panel illustrates representative SH2 domain structures (Suppressor of Cytokine Signalling
1273 1 and -2 and the PI3K alpha), and the bottom shows structural homology models of MGF 100
1274 members 1L, 1R, and I7L and I8L superimposed. The PHYRE2 algorithm (56) was used to predict
1275 models for MGF 100 members (Supplementary Table 2d), and the structures at the top were
1276 detected as the top hits for each of the MGF 100 models shown in the lower panel. (c) Structure-
1277 guided multiple sequence alignment of selected MGF 100 member models, alongside known SH2
1278 domain structures (annotated as SH2_name_PDB number).

1279

1280 Figure 11. Changes in the swine macrophage transcriptome upon ASFV GRG infection. (a) Major
1281 expression response profiles of the pig macrophage transcriptome. Late response genes are
1282 significantly deregulated (false discovery rate < 0.05) in one direction both between mock-infected
1283 (ctrl) and 16 hpi as well as between 5 and 16 hpi, but not between mock-infected and 5 hpi. Early
1284 response genes are significantly deregulated in one direction both between ctrl and 5 hpi as well as
1285 ctrl and 16 hpi, but not between 5 and 16 hpi. (b) Relationship of log fold changes (logFC) of TSS-
1286 derived gene expression levels of the total 9,384 swine genes expressed in macrophages between 5–
1287 16 hpi and ctrl–16 hpi. Colors correspond to the response groups from the panel a. (c) Relationship
1288 of log fold changes of TSS-derived gene expression levels of the total 9,384 swine genes expressed in
1289 macrophages between 5–16 hpi and ctrl–5 hpi. (d) MA plot of the TSS-derived gene expression levels
1290 between 5 and 16 hpi based on differential expression analysis with edgeR (108,115). (e)
1291 Representative overrepresented functional annotations of the upregulated (red) and downregulated
1292 (blue) macrophage genes following late transcription response (Benjamini-corrected p-value lower
1293 than 0.05). Numbers on the right to the bars indicate total number of genes from a given group
1294 annotated with a given annotation. (f) RT-PCR of four genes of interest indicated in (d). 'C' is the
1295 uninfected macrophage control, NTC is the Non Template Control for each PCR, excluding template
1296 DNA. See methods for primers used.

1297

1298 Figure 12. Protein expression at different times during infection of swine macrophages with ASFV-
1299 GRG. Two different batches of macrophages (S1 and S2) were infected with MOI 5 or left uninfected
1300 as a control (Ctrl) and at 0, 5 and 16hpi cellular extracts were collected and analysed via SDS-PAGE

1301 Western blot for the presence of ISG15 and γ-Tubulin as a protein loading control (a) and for the
1302 presence of viral protein P30 as control of ASFV infection (b). (c), (d) and (e) are the results from
1303 ELISAs for detection of porcine TNF-α, IL-8/CXCL8, and CCL2/MCP-1, respectively, in culture
1304 supernatants. Results are presented as 'Relative to control' values (y-axis of c-e) calculated by
1305 performing ELISAs in parallel for control and GRG infection at each timepoint.

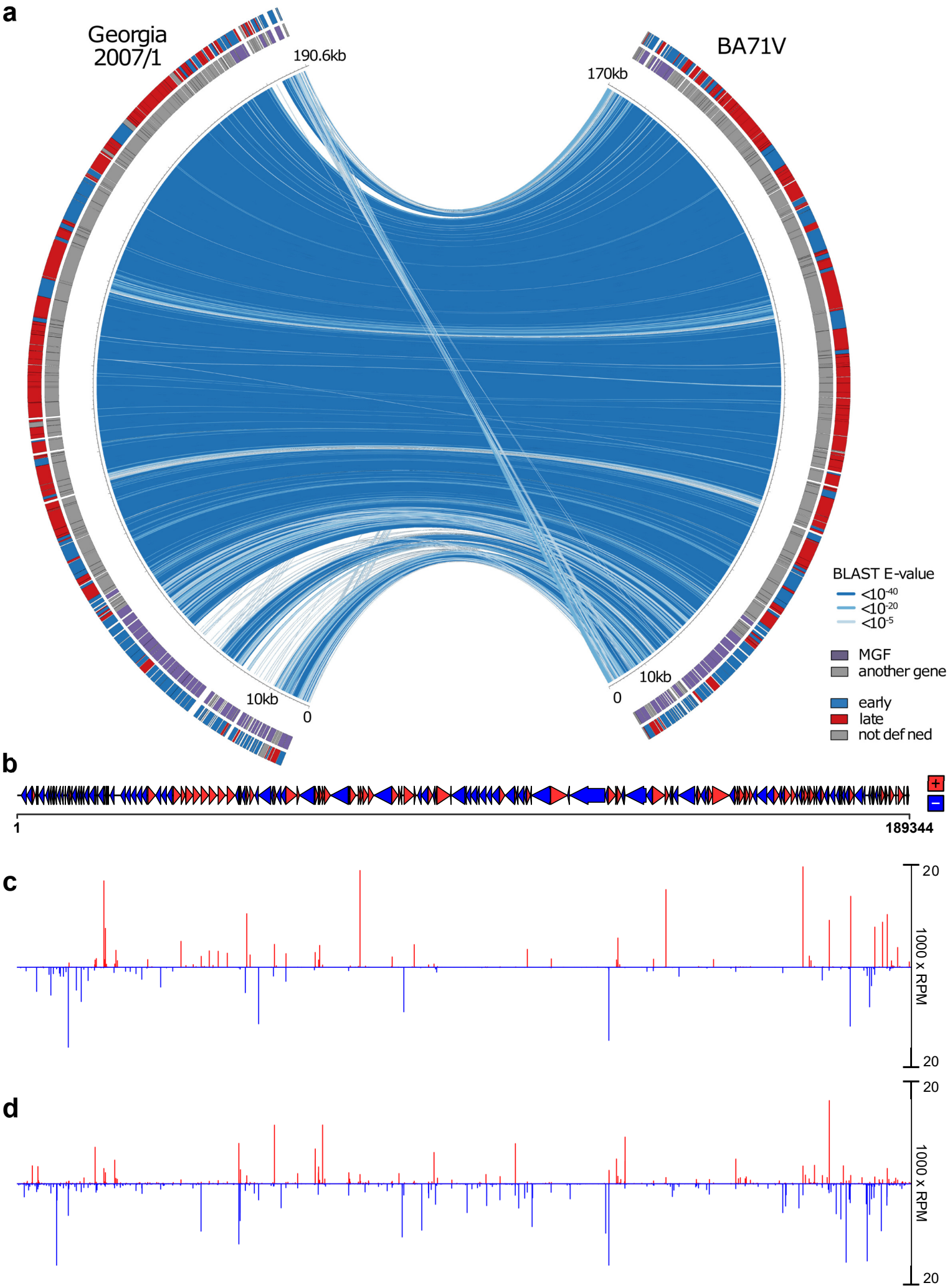
a
Georgia
2007/1
190.6kb
BA71V
170kb
10kb
0
10kb
0
BLAST E-value
<10-40
<10-20
<10-5
MGF
another gene
early
late
not def ned
b
1
189344
+
−
c
20
1000 x RPM
20
d
20
1000 x RPM
20

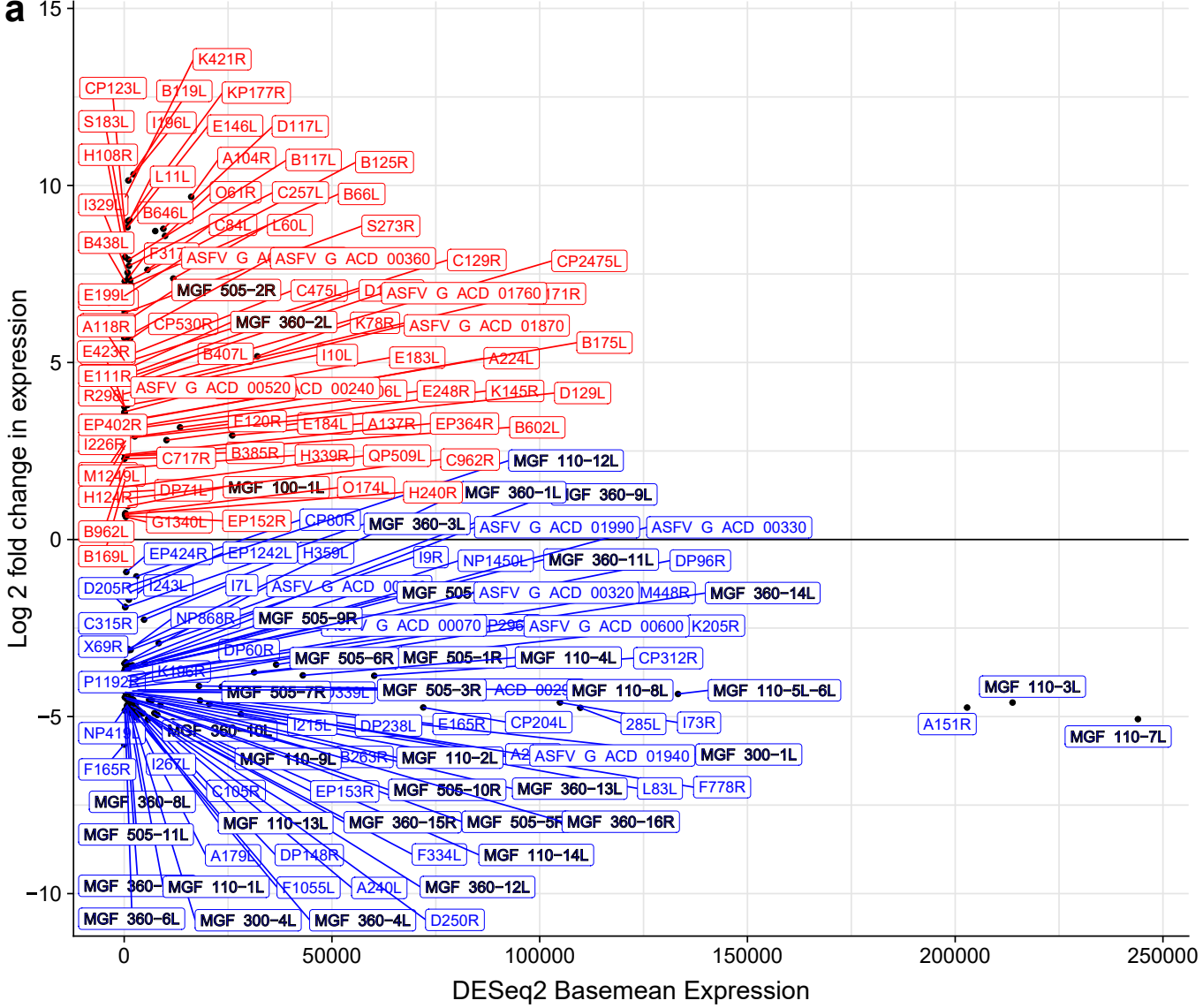
a
Log 2 fold change in expression
DESeq2 Basemean Expression
15
10
5
0
−5
−10
0
50000
100000
150000
200000
250000
K421R
CP123L
B119L
KP177R
S183L
I186L
E146L
D117L
H108R
A104R
B117L
B125R
L11L
O61R
C257L
B66L
I329L
B646L
C84L
L60L
S273R
B438L
ASFV G ACD 00360
C129R
CP2475L
E199L
MGF 505-2R
C475L
ASFV G ACD 01760
A118R
CP530R
MGF 360-2L
K78R
ASFV G ACD 01870
B175L
E423R
B407L
I10L
E183L
A224L
E111R
ASFV G ACD 00520
ASFV G ACD 00240
E248R
K145R
D129L
R298L
EP402R
E120R
E184L
A137R
EP364R
B602L
I226R
C717R
B385R
H339R
QP509L
C962R
MGF 110-12L
M1249L
MGF 100-1L
O174L
H240R
MGF 360-1L
MGF 360-9L
B962L
G1340L
EP152R
CP80R
MGF 360-3L
ASFV G ACD 01990
ASFV G ACD 00330
B169L
EP424R
EP1242L
H359L
I9R
NP1450L
MGF 360-11L
DP96R
D205R
I243L
I7L
MGF 505
ASFV G ACD 00320
M448R
MGF 360-14L
C315R
NP868R
MGF 505-9R
ASFV G ACD 00070
ASFV G ACD 00600
K205R
X69R
DP60R
MGF 505-6R
MGF 505-1R
MGF 110-4L
CP312R
P1192R
MGF 505-7R
MGF 505-3R
MGF 110-8L
MGF 110-5L-6L
MGF 110-3L
A151R
MGF 110-7L
NP419L
I215L
DP238L
E165R
CP204L
285L
I73R
F165R
MGF 110-9L
MGF 110-2L
ASFV G ACD 01940
MGF 300-1L
C105R
EP153R
MGF 505-10R
MGF 360-13L
L83L
F778R
MGF 360-8L
MGF 110-13L
MGF 360-15R
MGF 505-5R
MGF 360-16R
MGF 505-11L
A179L
DP148R
F334L
MGF 110-14L
MGF 110-1L
F1055L
A240L
MGF 360-12L
MGF 360-6L
MGF 300-4L
MGF 360-4L
D250R

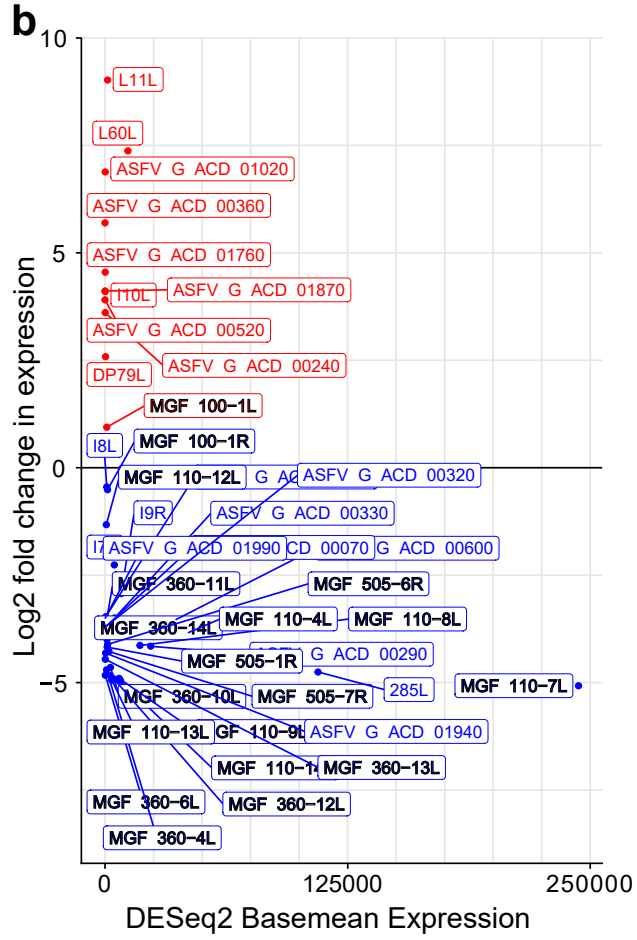
b
Log2 fold change in expression
DESeq2 Basemean Expression
10
5
0
−5
0
125000
250000
L11L
L60L
ASFV G ACD 01020
ASFV G ACD 00360
ASFV G ACD 01760
I10L
ASFV G ACD 01870
ASFV G ACD 00520
ASFV G ACD 00240
DP79L
MGF 100-1L
I8L
MGF 100-1R
MGF 110-12L
ASFV G ACD 00320
I9R
ASFV G ACD 00330
ASFV G ACD 01990
ASFV G ACD 00600
MGF 360-11L
MGF 505-6R
MGF 360-14L
MGF 110-4L
MGF 110-8L
MGF 505-1R
285L
MGF 110-7L
MGF 360-10L
MGF 505-7R
MGF 110-13L
ASFV G ACD 01940
MGF 360-13L
MGF 360-6L
MGF 360-12L
MGF 360-4L

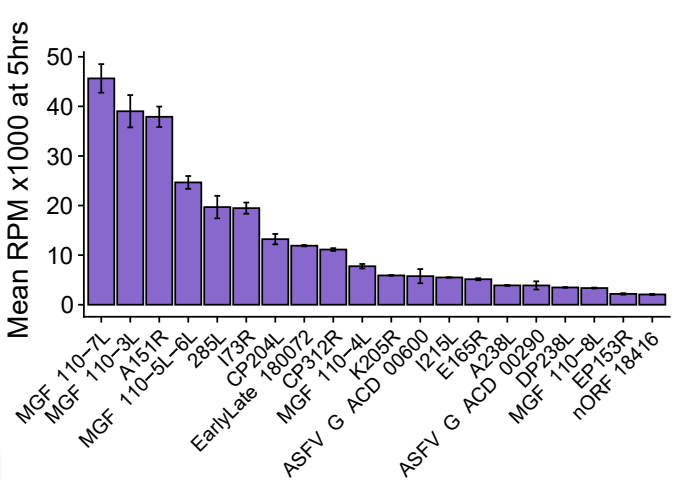
c
Mean RPM x1000 at 5hrs
50
40
30
20
10
0
MGF 110-7L
MGF 110-3L
A151R
MGF 110-5L-6L
285L
I73R
CP204L
EarlyLate 180072
CP312R
MGF 110-4L
K205R
ASFV G ACD 00600
I215L
E165R
A238L
ASFV G ACD 00290
DP238L
MGF 110-8L
EP153R
nORF 18416

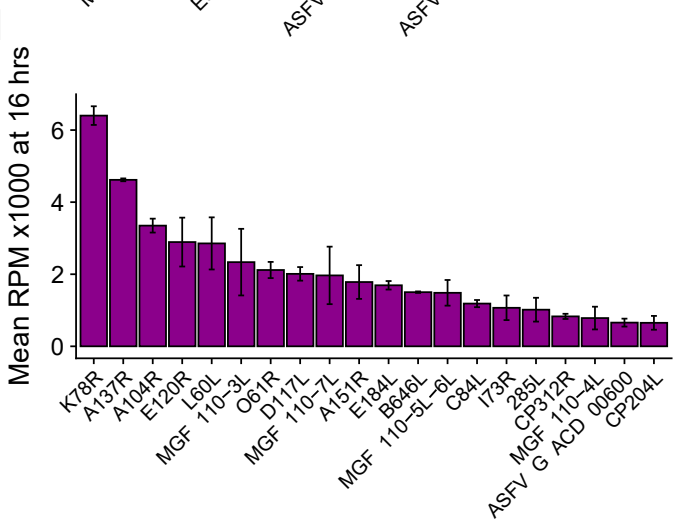
d
Mean RPM x1000 at 16 hrs
6
4
2
0
K78R
A137R
A104R
E120R
L60L
MGF 110-3L
O61R
D117L
MGF 110-7L
A151R
E184L
B646L
MGF 110-5L-6L
C84L
I73R
285L
CP312R
MGF 110-4L
ASFV G ACD 00600
CP204L

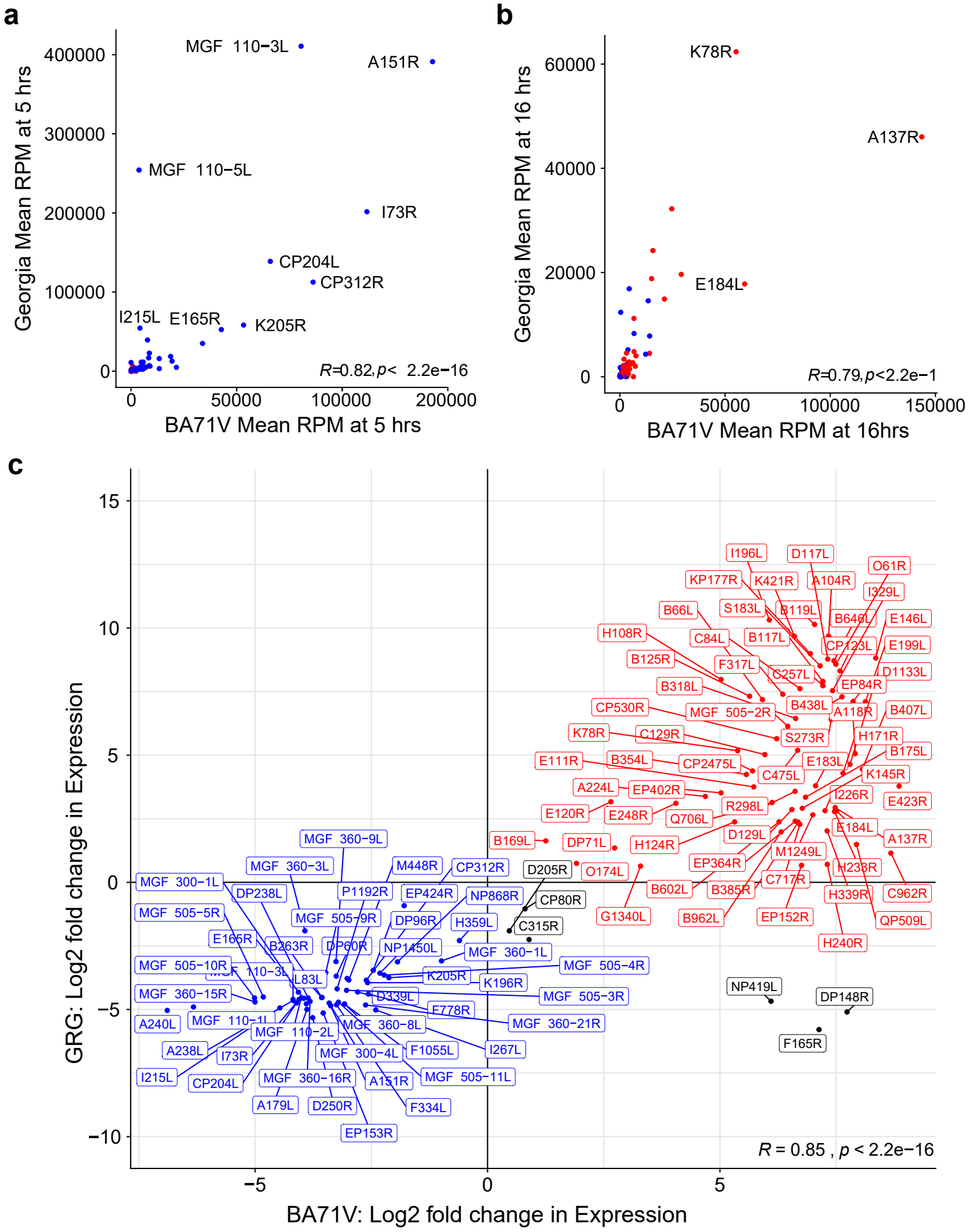
a
Georgia Mean RPM at 5 hrs
BA71V Mean RPM at 5 hrs
MGF 110−3L
A151R
MGF 110−5L
I73R
CP204L
CP312R
I215L
E165R
K205R
R=0.82, p< 2.2e−16
b
Georgia Mean RPM at 16 hrs
BA71V Mean RPM at 16hrs
K78R
A137R
E184L
R=0.79, p<2.2e−1
c
GRG: Log2 fold change in Expression
BA71V: Log2 fold change in Expression
R = 0.85 , p < 2.2e−16

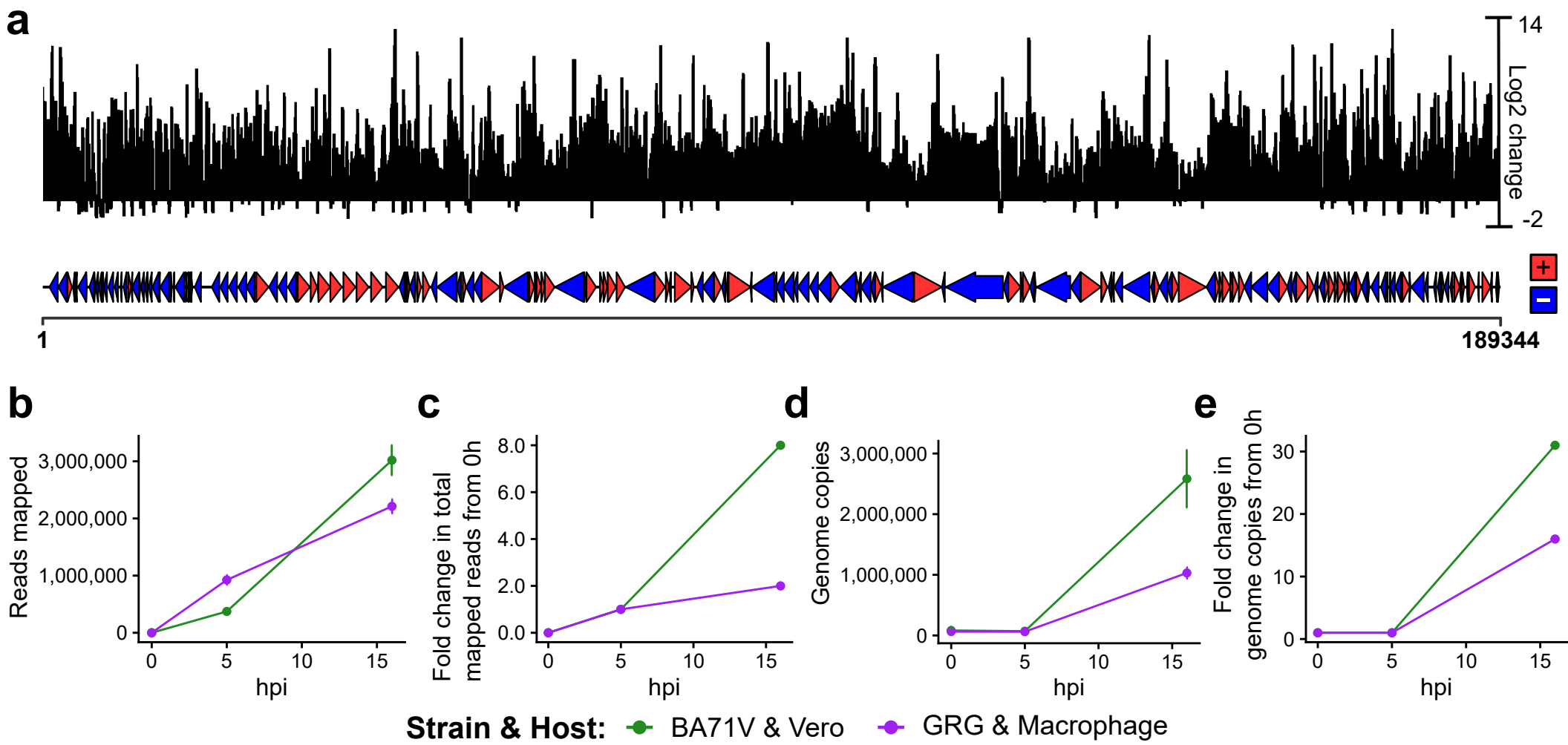
a
14
Log2 change
-2
+
−
1
189344
b
Reads mapped
3,000,000
2,000,000
1,000,000
0
0
5
10
15
hpi
c
Fold change in total mapped reads from 0h
8.0
6.0
4.0
2.0
0.0
0
5
10
15
hpi
d
Genome copies
3,000,000
2,000,000
1,000,000
0
0
5
10
15
hpi
e
Fold change in genome copies from 0h
30
20
10
0
0
5
10
15
hpi
Strain & Host:
BA71V & Vero
GRG & Macrophage

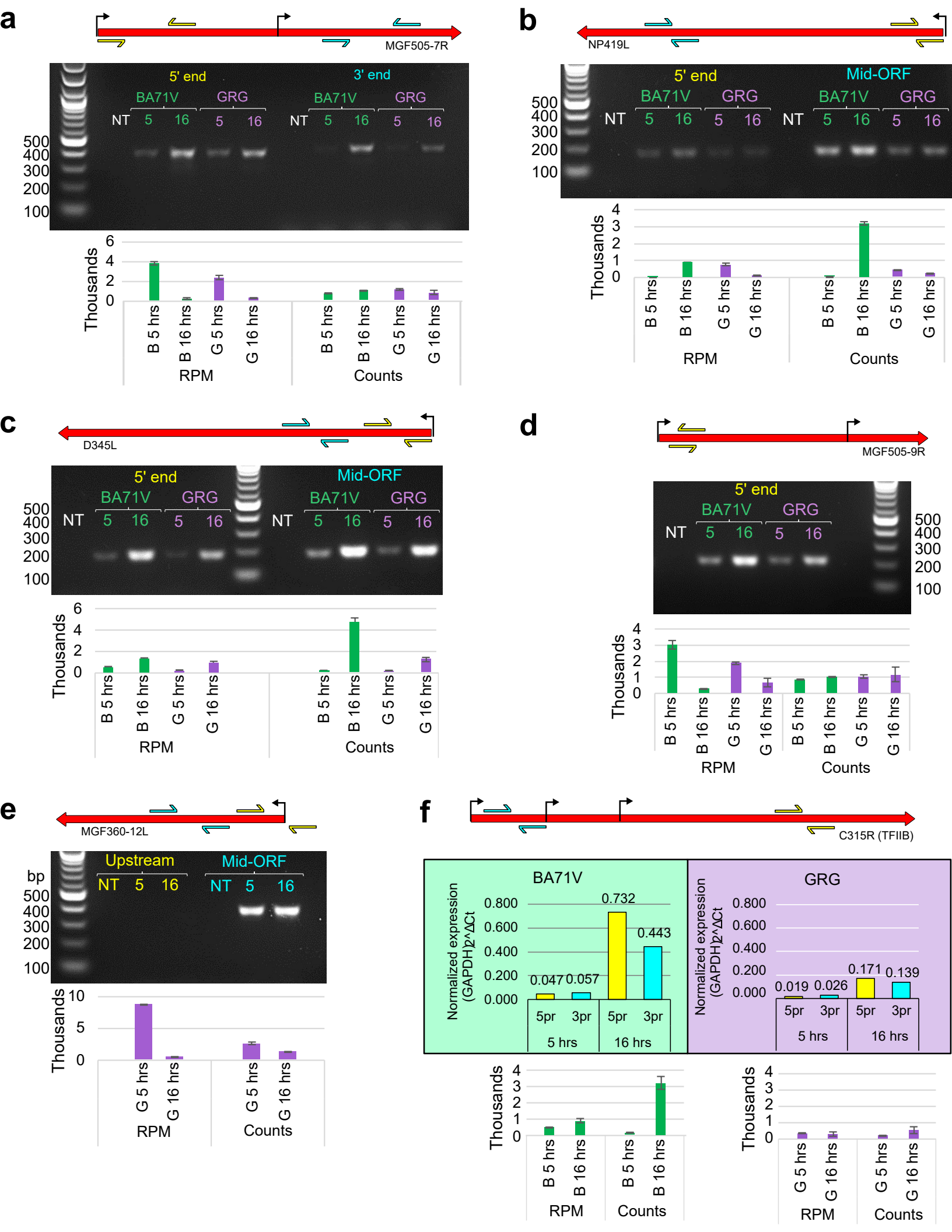
a
MGF505-7R
5' end
3' end
BA71V
GRG
NT
5
16
500
400
300
200
100
Thousands
6
4
2
0
B 5 hrs
B 16 hrs
G 5 hrs
G 16 hrs
RPM
Counts
b
NP419L
5' end
Mid-ORF
3
1
c
D345L
d
MGF505-9R
e
MGF360-12L
Upstream
Mid-ORF
bp
10
5
f
C315R (TFIIB)
Normalized expression (GAPDH)2^ΔCt
0.800
0.600
0.400
0.200
0.000
0.047
0.057
0.732
0.443
0.019
0.026
0.171
0.139
5pr
3pr
5 hrs
16 hrs

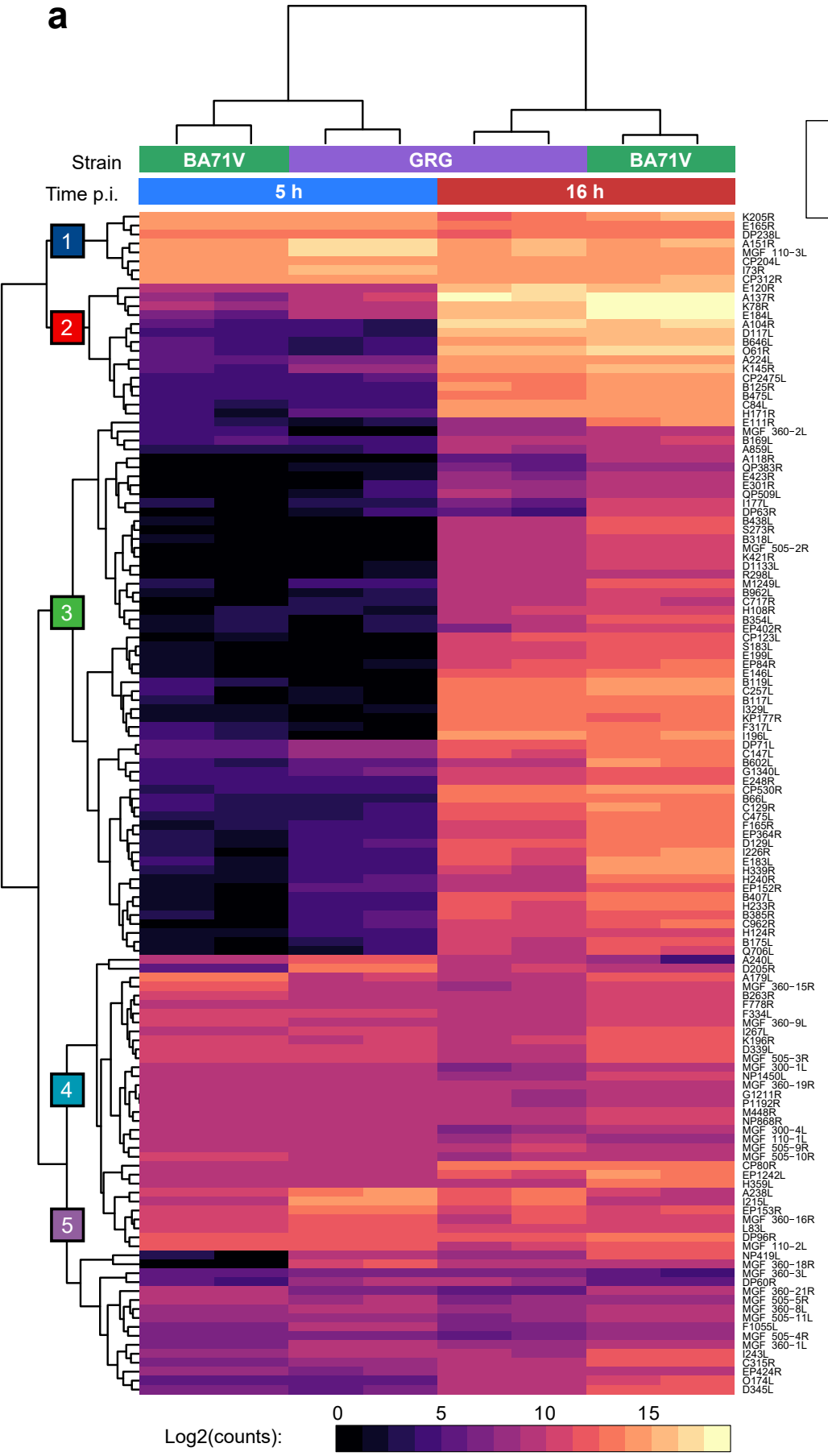

b

	Counts 5h	Counts 16h	Cluster pattern
1	high	high	both high (H-H)
2	low	high	low to high (L-H)
3	low	mid	low to mid (L-M)
4	mid	mid	both mid (M-M)
5	low-mid	low-mid	both low-mid (LM-LM)

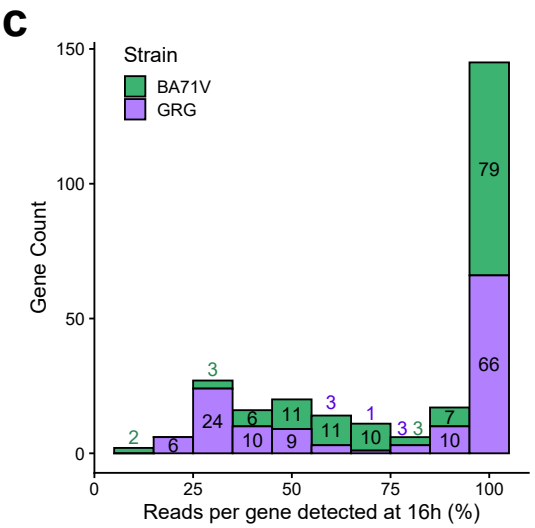

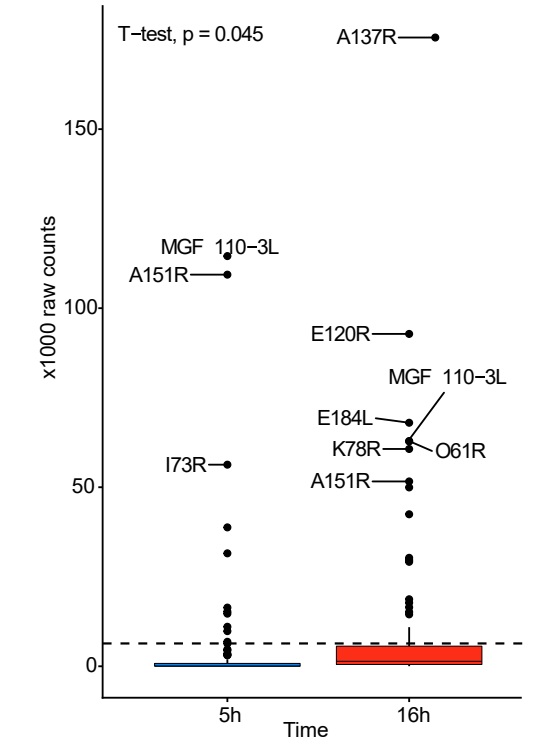

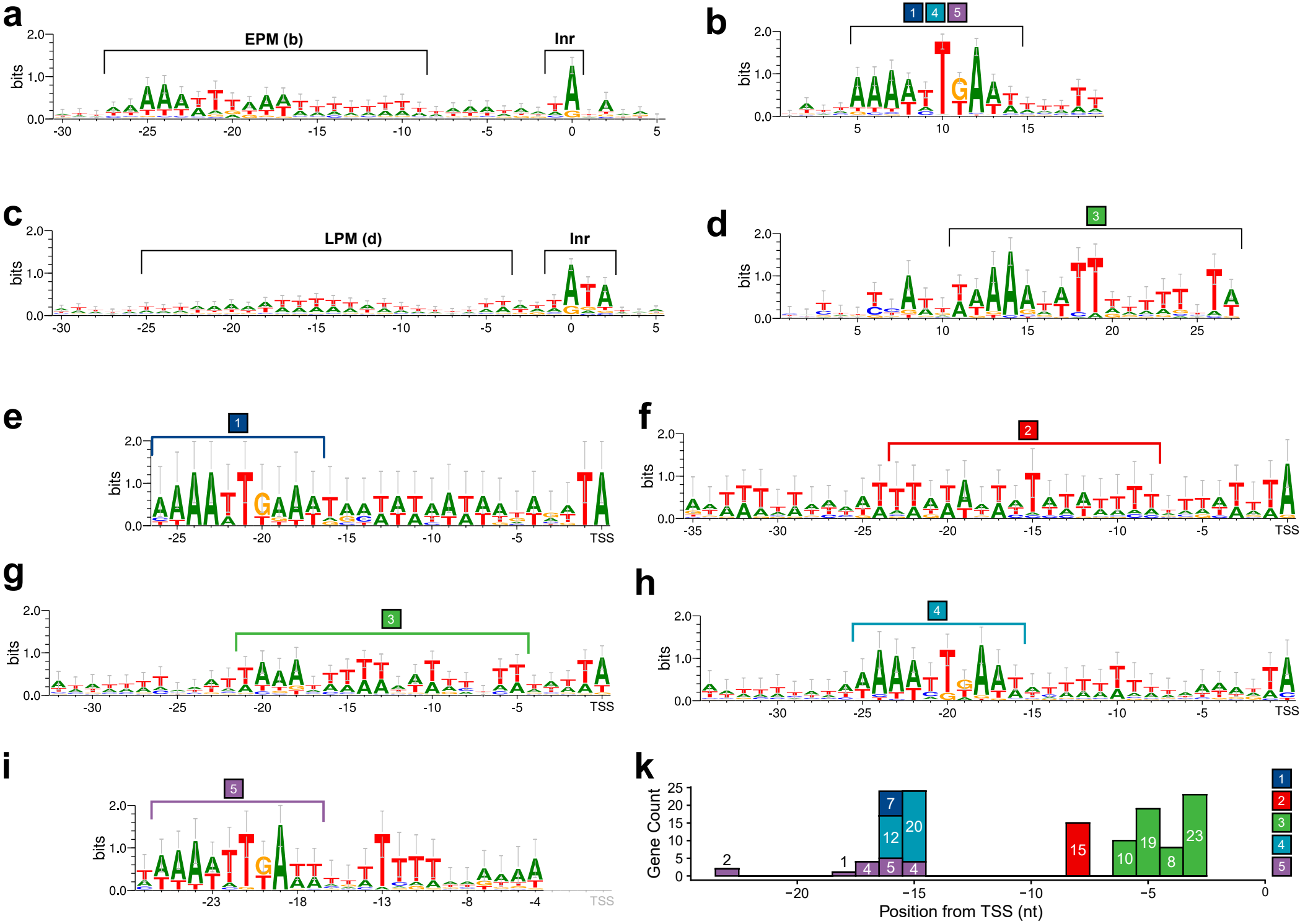
a
EPM (b)
Inr
b
c
LPM (d)
Inr
d
e
f
g
h
i
k
bits
Gene Count
Position from TSS (nt)
TSS

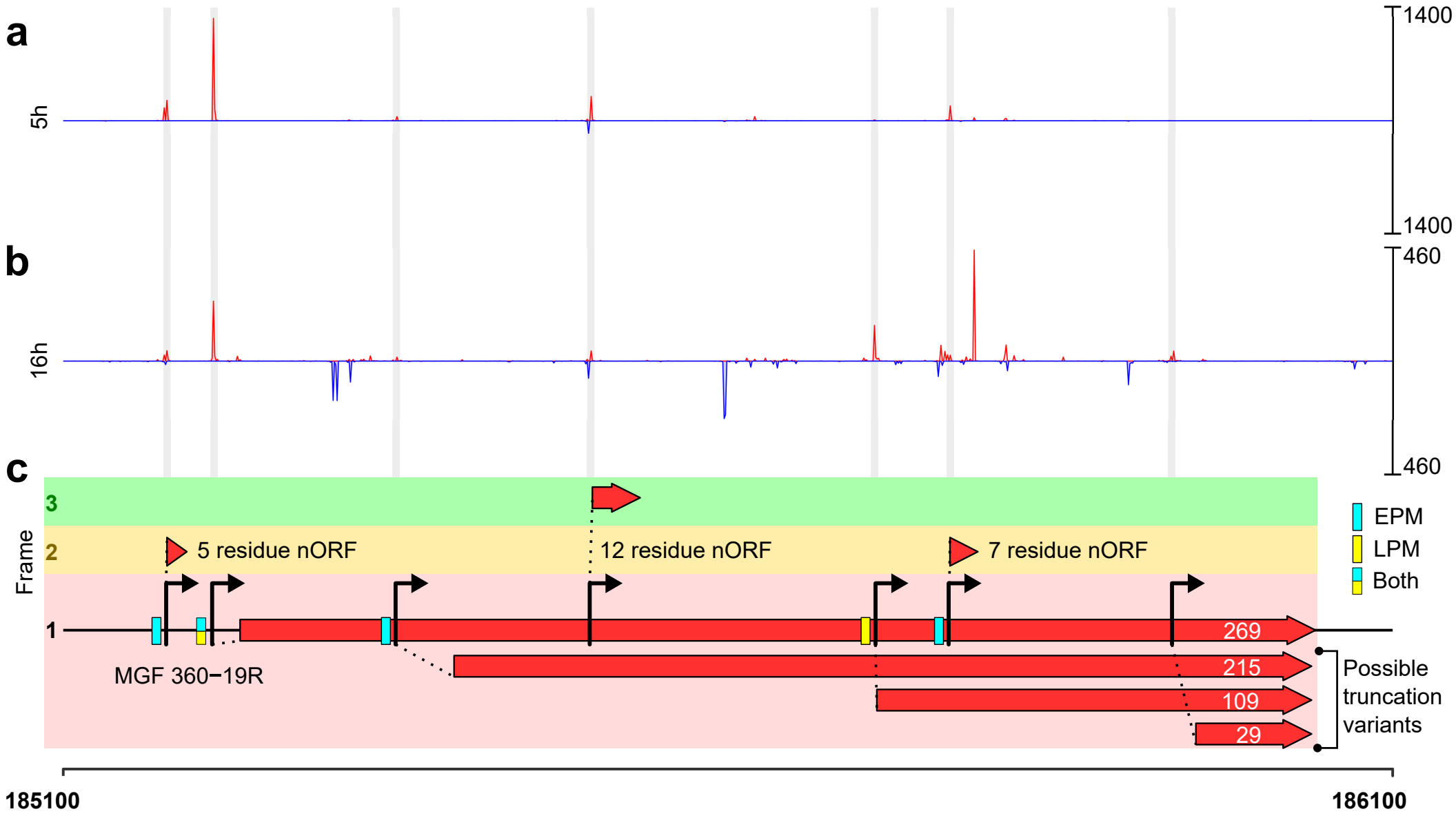
a
5h
1400
1400
b
16h
460
460
c
Frame
3
2
1
5 residue nORF
12 residue nORF
7 residue nORF
EPM
LPM
Both
269
215
109
29
MGF 360−19R
Possible truncation variants
185100
186100

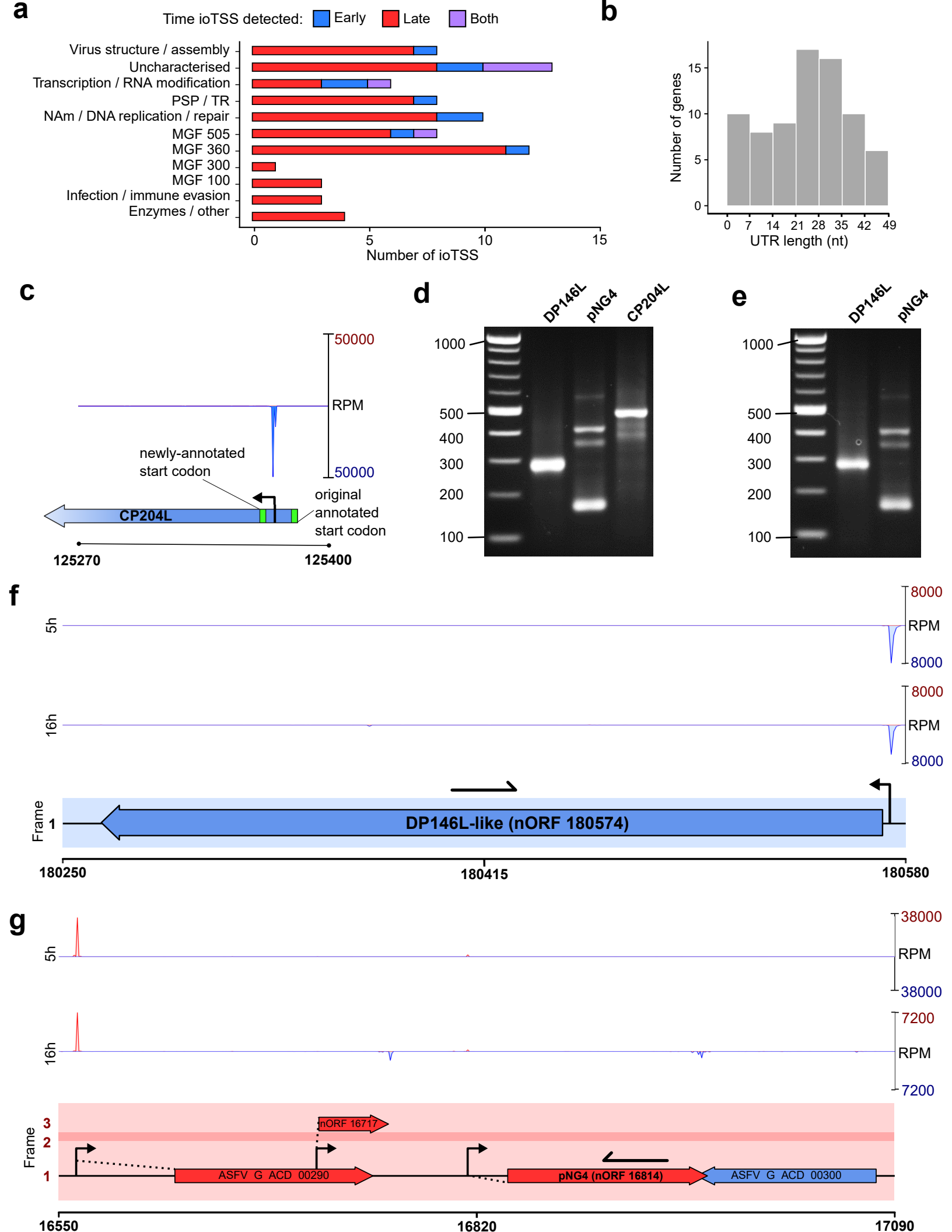
a
Time ioTSS detected:
Early
Late
Both
Virus structure / assembly
Uncharacterised
Transcription / RNA modification
PSP / TR
NAm / DNA replication / repair
MGF 505
MGF 360
MGF 300
MGF 100
Infection / immune evasion
Enzymes / other
0
5
10
15
Number of ioTSS
b
Number of genes
0
5
10
15
0
7
14
21
28
35
42
49
UTR length (nt)
c
50000
RPM
50000
newly-annotated
start codon
original
annotated
start codon
CP204L
125270
125400
d
DP146L
pNG4
CP204L
1000
500
400
300
200
100
e
DP146L
pNG4
1000
500
400
300
200
100
f
5h
8000
RPM
8000
16h
8000
RPM
8000
Frame
1
DP146L-like (nORF 180574)
180250
180415
180580
g
5h
38000
RPM
38000
16h
7200
RPM
7200
Frame
3
2
1
nORF 16717
ASFV_G_ACD_00290
pNG4 (nORF 16814)
ASFV_G_ACD_00300
16550
16820
17090

a

Genotype	ASFV strain	Pathogenic	Source
I	BA71V	N	NC_001659.2
I	BA71	Y	NC_044942
I	Portugal, OURT88/3	N	AM712240.1
I	Benin 97/1	Y	AM712239.1
II	Georgia 2007/1	Y	FR682468.2
II	Georgia 2007/1-VP110	N	Krug *et al.*
II	China/2018/AnhuiXCGQ	Y	MK128995.1
IX	Ken05/Tk1	Y	KM111294.1
X	Kenya 1950	Y	AY261360.1

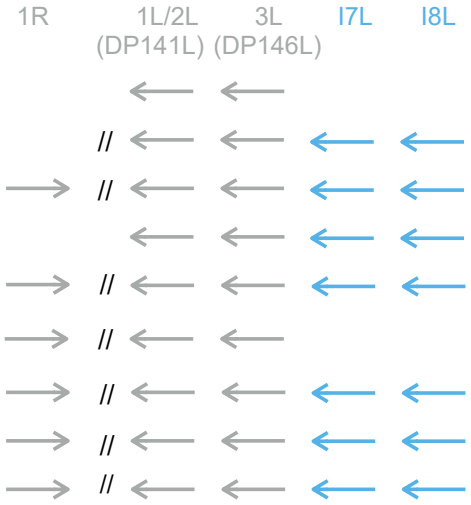

b

PDB ID: 2C9W .A
Suppressor of Cytokine Signalling 1

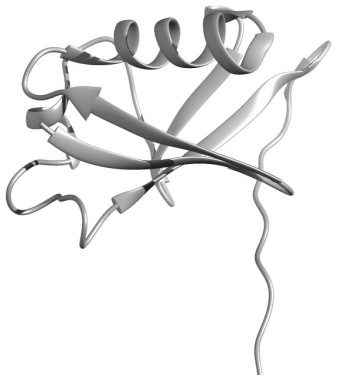

PDB ID: 6C5X .D
Suppressor of Cytokine Signalling 2

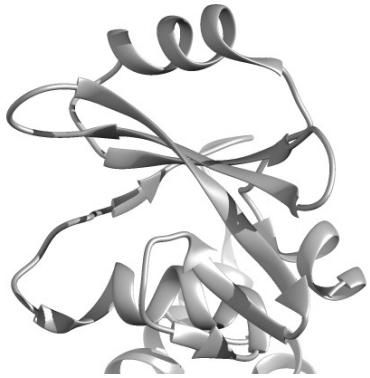

PDB ID: 4L1B .B
PIK3 regulatory subunit alpha

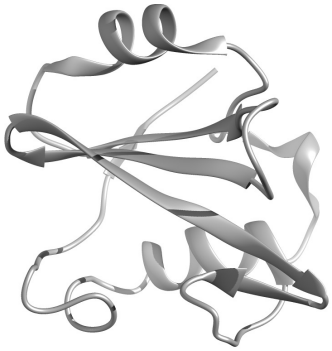

Model: MGF 100-1L (GRG)
Template PDB ID: 2C9W .A

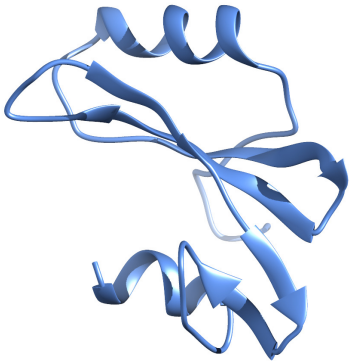

Model: MGF 100-1R (GRG)
Template PDB ID: 6C5X .D

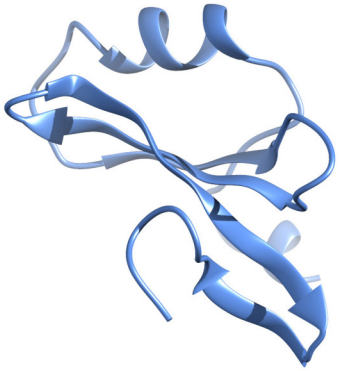

Model: I7L & I8L (GRG)
Template PDB ID: 4L1B .B

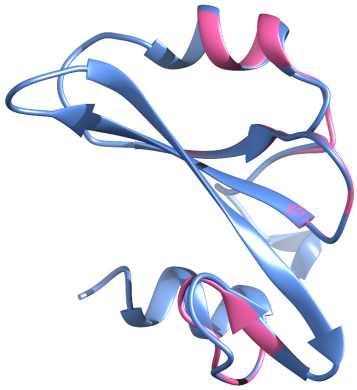

c

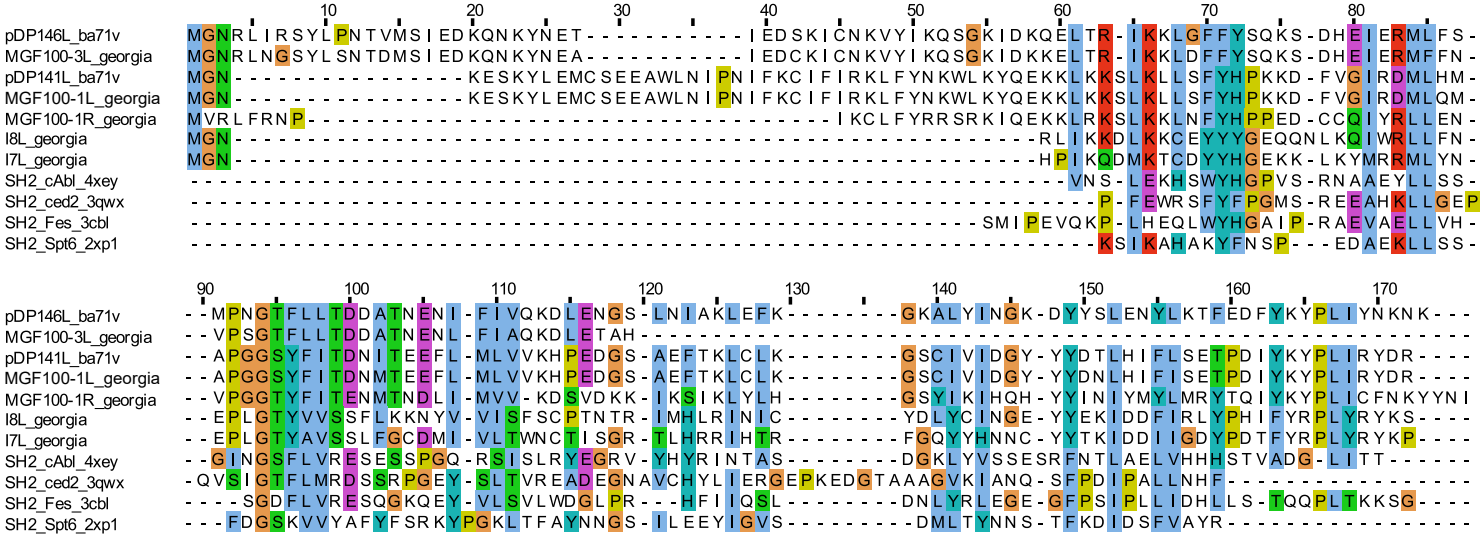

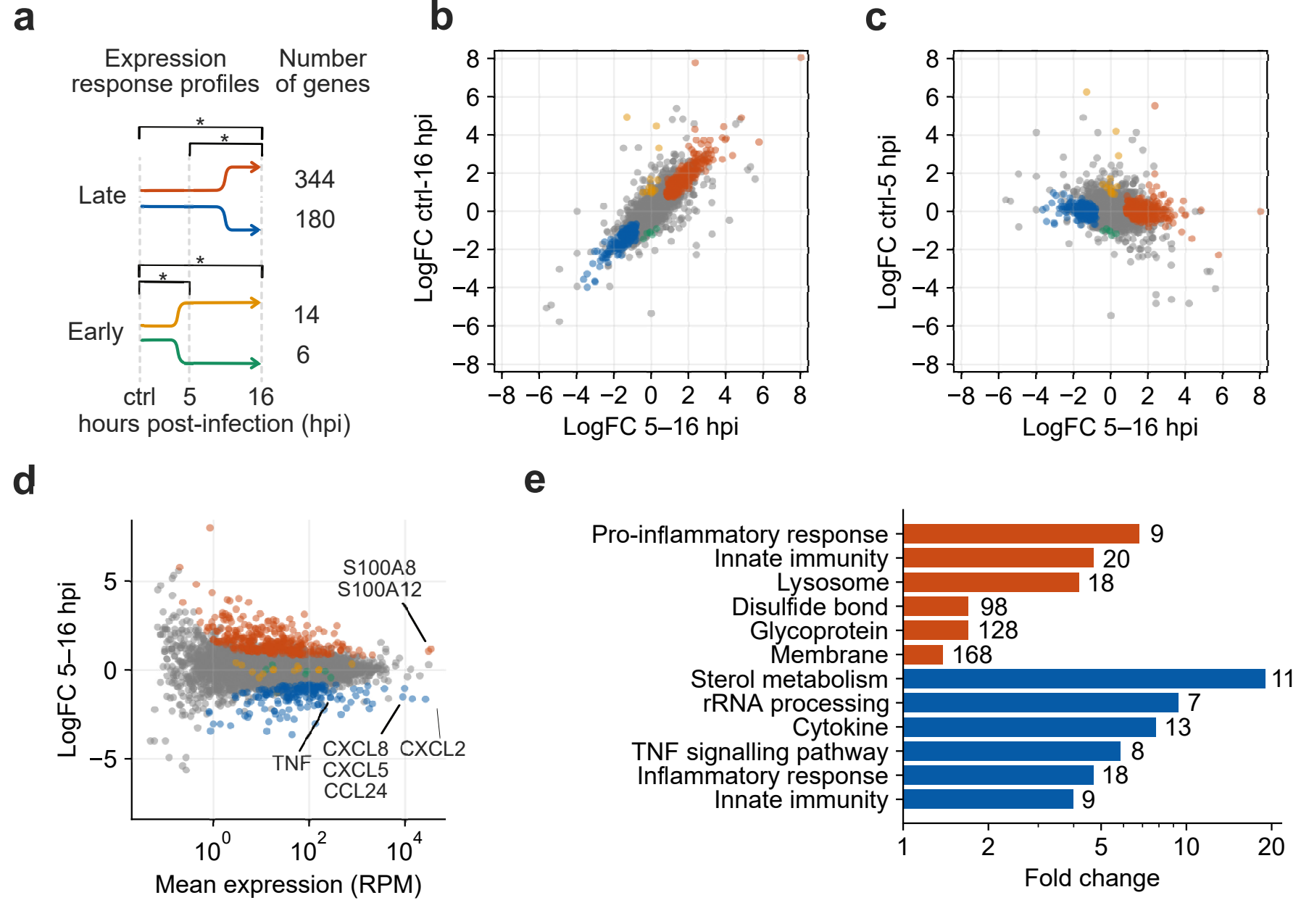
a
Expression response profiles
Number of genes
Late
344
180
Early
14
6
ctrl
5
16
hours post-infection (hpi)
b
LogFC ctrl-16 hpi
LogFC 5–16 hpi
c
LogFC ctrl-5 hpi
LogFC 5–16 hpi
d
LogFC 5–16 hpi
Mean expression (RPM)
S100A8
S100A12
TNF
CXCL8
CXCL5
CCL24
CXCL2
e
Pro-inflammatory response 9
Innate immunity 20
Lysosome 18
Disulfide bond 98
Glycoprotein 128
Membrane 168
Sterol metabolism 11
rRNA processing 7
Cytokine 13
TNF signalling pathway 8
Inflammatory response 18
Innate immunity 9
Fold change

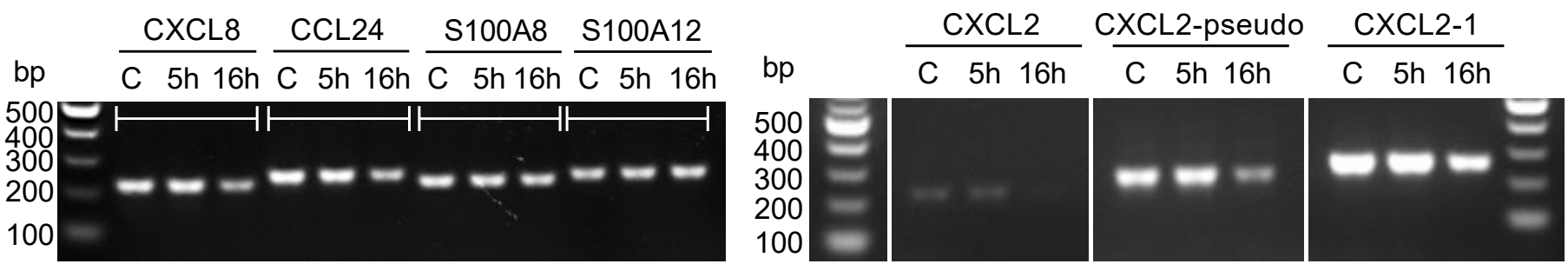
f
CXCL8
CCL24
S100A8
S100A12
bp
C 5h 16h
500
400
300
200
100
CXCL2
CXCL2-pseudo
CXCL2-1

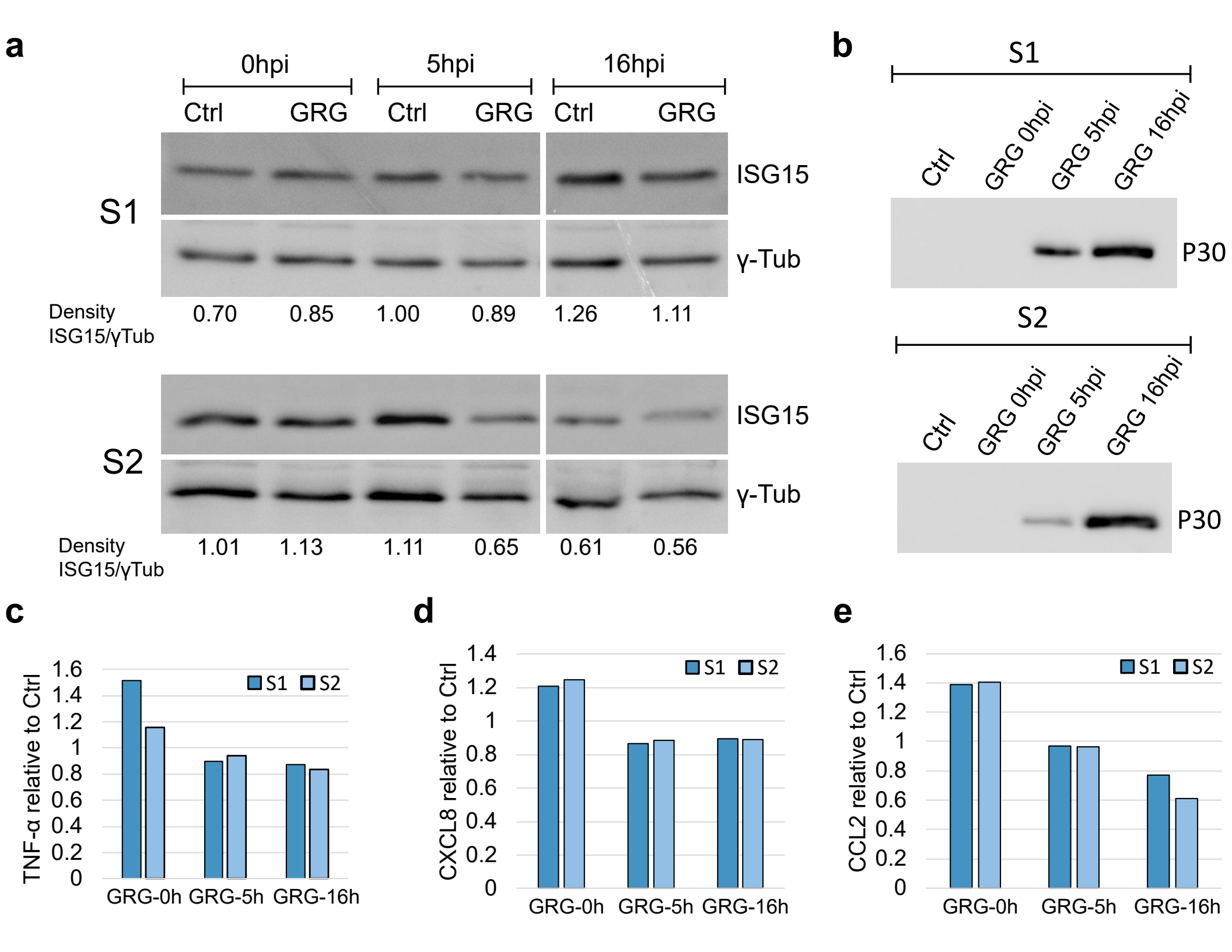
a
0hpi
5hpi
16hpi
Ctrl
GRG
Ctrl
GRG
Ctrl
GRG
S1
ISG15
γ-Tub
Density ISG15/γTub
0.70
0.85
1.00
0.89
1.26
1.11
S2
ISG15
γ-Tub
Density ISG15/γTub
1.01
1.13
1.11
0.65
0.61
0.56
b
S1
Ctrl
GRG 0hpi
GRG 5hpi
GRG 16hpi
P30
S2
Ctrl
GRG 0hpi
GRG 5hpi
GRG 16hpi
P30
c
TNF-α relative to Ctrl
S1
S2
GRG-0h
GRG-5h
GRG-16h
d
CXCL8 relative to Ctrl
S1
S2
GRG-0h
GRG-5h
GRG-16h
e
CCL2 relative to Ctrl
S1
S2
GRG-0h
GRG-5h
GRG-16h